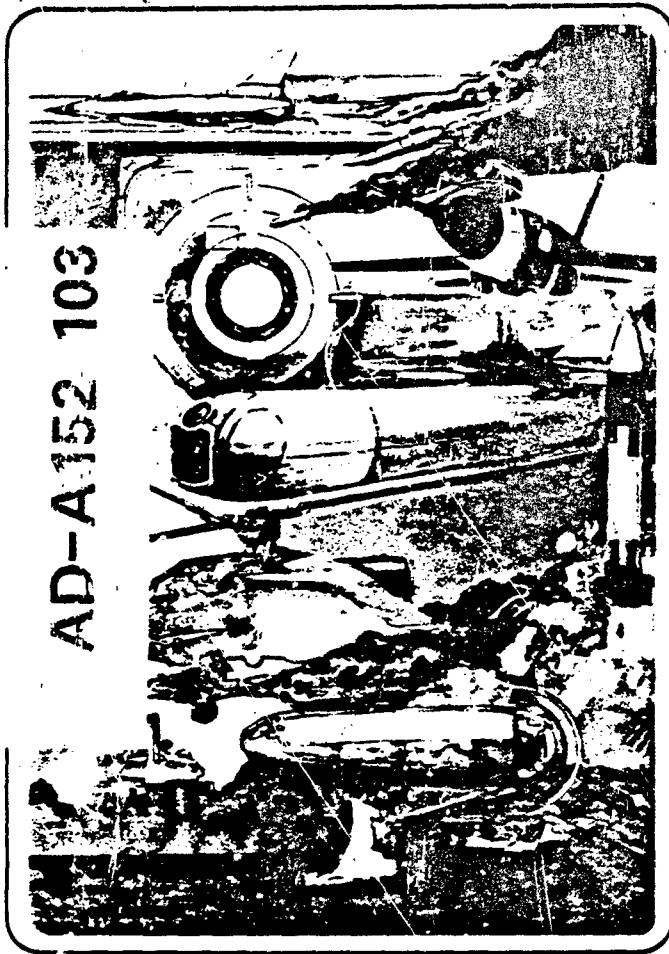


FIR 1026

(2)



AD-A152 103

MARTIN MARIETTA ORLANDO AEROSPACE

DTIC FILE COPY

Reproduced From
Best Available Copy

DTIC
ELECTE

APR 3 1985

S
A

This document has been approved
for public release and sale; its
distribution is unlimited.

MARTIN MARIETTA

20000807036

85 03 12 080

FINAL INTERIM MANUFACTURING METHODS REPORT

DATA ITEM A003
CONTRACT DAAH-01-80-C-1567

CONTRACT PERIOD OF PERFORMANCE
29 August 1980 through 31 August 1981

Submitted By:

Martin Marietta Orlando Aerospace

Orlando, Florida

R. J. Schwalbe
W. F. Prater
F. H. Koo
J. C. Winkler

Submitted To:

U.S. Army Missile Command
Redstone Arsenal, Alabama

ATTN: DRSMI-RLM
ATTN: DRSMI-RST
ATTN: DRSMI-IYO
ATTN: ACO
ATTN: DRCPM

MANUFACTURING METHODS AND TECHNOLOGY
PROJECT FOR PRODUCTION OF
LOW COST MISSILE VANES

OR 16,579

February 1982

Accession Box
TITLE: ✓
EPIC: ✓
Unprocessed
By: *Auto file*
Distribution/
Availability: ✓
Date: *AI*



CONTENTS

Introduction and Background 1

1.0 Conclusions and Recommendations 3

2.0 Technical Discussion 5

 2.1 Task I - Planning 7

 2.2 Task II - Material and Mechanical
 Property Evaluation 7

 2.2.1 Composite Skin Requirements 9

 2.2.2 Adhesive and Honeycomb Core Evaluation 11

 2.3 Task III - Design 13

 2.3.1 Structural Analysis 13

 2.3.2 Thermal Analysis 17

 2.3.3 Static Test Plan 20

 2.4 Task IV - Tool Design and Fabrication 26

 2.5 Task V - Process Demonstration 29

 2.5.1 Fabrication 30

 2.5.2 Static Test Results 38

APPENDIX A Composite Air Vane Thermal Analysis 43

ILLUSTRATIONS

2-1	Major Tasks are Interdependent	5
2-2	Composite Air Vane Basic Effort	6
2.2-1	Low Cost Missile Vane	8
2.2-2	Low Cost Composite Air Vane Configuration	8
2.2.1-1	Air Vane Structural Design Requirements	9
2.2.1-2	Air Vane Torque Box	10
2.2.2 1-1	Double-Lap Shear Specimen Configuration	11
2.2.2.2-1	Honeycomb Specimen Configuration	12
2.3.1-1	Finite Element Model - Steel Base	14
2.3.1-2	Finite Element Model - Shell	15
2.3.1-3	Finite Element Model - Honeycomb Core	16
2.3.1-4	Air Vane Structural Design Requirements	16
2.3.2-1	RV Fin Leading Edge Local Pressure During Reentry	18
2.3.2-2	RV Fin Leading Edge Cold Wall Heat Flux During Reentry .	18
2.3.2-3	RV Fin Side Panel Cold Wall Heat Flux During Reentry . .	19
2.3.2-4	RV Fin Bottom Gap Augmented Cold Wall Flux During Reentry	19
2.3.3-1	RV Design Limit Load	21
2.3.3-2	Composite Air Vane Test Load Distribution	21
2.3.3-3	Static Test Fixture Load Arrangement	23
2.3.3-4	Location of Deflection Measurement	23

ILLUSTRATIONS

2.3.3-5	Locations of Rosette Strain Gages	23
2.3.3-6	Static Test Article in Test Fixture	24
2.4-1	Matched, Metal Die Compression Mold for Net Molding of Cocured Structure	26
2.4-2	Matched Metal Die Bonding Assembly for Landing Honeycomb Torque Box Assembly to Cocured Structure	27
2.4-3	Graphite Epoxy Substructure Staging Tool and Templates	28
2.4-4	Ablative Side Panels, Back Panel and Bottom Panel Templates	28
2.4-5	Leading Edge Folding Wedge and Final Staging Tool	29
2.5.1-1	Tapewrapping of Ablative Heat Shield for Side, Bottom, and Back Panels	31
2.5.1-2	Silica Phenolic Leading Edge Fabrication Process	33
2.5.1-3	Folding Leading Edge Preform and Final Staging	34
2.5.1-4	Graphite Epoxy Substructure Lay Up	35
2.5.1-5	Net Molded and Cocured Structure	35
2.5.1-6	Honeycomb Core Prior to Final Machining	36
2.5.1-7	Honeycomb Core Positioned in Pocket Area of Torque Box	36
2.5.1-8	Honeycomb Core Bonded and Machined in Torque Box	37
2.5.1-9	Prefit for Final Bonding of Honeycomb Torque Box to Cocured Structure	37
2.5.1-10	Final Composite Air Vane Assembly	38
2.5.1-11	Process Flow Plan	38
2.5.2-1	DCDT Locations	39
2.5.2-2	Strain Gage Locations	40

A-1	RV Vane Leading Edge Local Pressure	46
A-2	Vane Leading Edge Cold Wall Heat Flux	47
A-3	Silica Phenolic Rain Erosion Resistance	48
A-4	RV Vane Deflection and Angle of Attack Versus Time	49
A-5	RV Vane Side Panel Cold Wall Heat Flux	49
A-6	Rain Erosion Resistance	50
A-7	Root Chord Cold Wall Heat Flux	52
A-8	Three Dimensional Root Chord Casting	52
A-9	RV Fin Trailing Edge Cold Wall Heat Flux	53
A-10	Vane Leading Edge Surface Temperature	54
A-11	Leading Edge Backside Temperature Response	55
A-12	Leading Edge Total Recession	55
A-13	Vane Side Panel Ablative Recession	56
A-14	Side Panel Bondline Thermal Recession	57
A-15	Root Chord Total Thermal Recession	58
A-16	Root Chord Bondline Temperature Response	58
A-17	Graphite Epoxy/Root Chord Stainless Steel	59
A-18	Trailing Edge Bondline Temperature Response	69

TABLES

2.2.1-I	Graphite Epoxy Skin Material Candidates	9
2.2.1-II	17-4PH Metallic Structure Deflection Results	10
2.2.2.1-I	First Adhesive Test	11
2.2.2.1-II	Second Adhesive Test	12
2.2.2.2-I	Honeycomb Core Shear Tests	13
2.3.1-I	Material Properties Input	14
2.3.1-II	Honeycomb Properties	14
2.3.1-III	Air Vane Deflection Under Maximum Load Conditions	15
2.3.2-I	Composite Air Vane Heatshield Sizing Summary	20
2.3.3-I	Static Test Loading Profile	25
2.5.2-I	Deflection at 100 Percent Design Limit Load (DLL)	339
2.5.2-II	Stress Components - Test	40
2.5.2-III	Stress Components - Analysis	41
A-I	Silica Phenolic Thermal Properties	47
A-II	Rubber Modified Silica Phenolic (RMSP-1/2) Thermal Properties	50
A-III	Graphite/Epoxy Thermal Properties	51
A-IV	Composite Air Vane Heatshield Sizing Summary	61

INTRODUCTION AND BACKGROUND

Graphite fiber/reinforced epoxy resin composites have been developed and fabricated for aerospace vehicle structural applications since the early 1960s. Early applications were oriented toward secondary structures to establish confidence and reliability under a service environment. The advances made in the past decade have caused acceptance of composite materials for primary structures on aircraft, missiles, and space vehicles. During the 1970s, the cost of these composite structures began to be reduced to be cost competitive with metal structures.

→ Martin Marietta's experience with ablative air vanes dates to the 1950s with the development of the Pershing I missile. During the 1960s, Martin Marietta continued such development on the Sprint and SAM-D (Patriot) missiles. In 1969, Martin Marietta Orlando Aerospace demonstrated net molding and primary bonding on the Sprint air vane, and also the potential cost savings during manufacturing. However, the high pressures required for molding caused excessive deflections of the metallic substructure, and the process was not implemented. This problem was eliminated later by net molding the composite structure and post-bonding it to the substructure.

↘ Pershing II (PII), started in the 1970s, used proven air vane technologies developed for Sprint. The Pershing vanes consisted of metallic substructures, designed to accept the air loads, and heat shields, designed to protect the substructures from severe aerodynamic heating and rain erosion.

The main cost driver for air vane fabrication, such as for Pershing II and Patriot, was the need to separately fabricate and apply heat shield panels to the basic metallic structure, which is a costly operation. To avoid this cost, Martin Marietta fabricated the heat shield and structural composite in a single cocured net molded operation. In 1979, Martin Marietta Orlando Aerospace demonstrated cocuring ablative materials to graphite/ polyimide skins, which were then bonded to a steel substructure.

By simplifying the then present casting substructure to a simpler torque box and by using numerical control machining techniques, Martin Marietta realized additional cost savings. Further, because a heat shield was used on the torque box, epoxy could be used as the composite matrix material instead of the polyimide, thereby reducing processing cost and criticality. Martin Marietta Orlando Aerospace has demonstrated all the subtechnologies required to obtain this cost reduction in advanced air vane fabrication. The objective of this program was to combine these subtechnologies into a complete advanced air vane manufacturing technology capable of reducing the cost and increasing the performance of parts currently made from metallics by using fiber-reinforced composites.

1.0 CONCLUSIONS AND RECOMMENDATIONS

There are four conclusions to be drawn from the results of this program:

- 1 Composite air vanes fabricated in accordance with baseline Pershing II metallic air vane structural requirements are more than adequate, as demonstrated by the static tests.
- 2 The net molding and cocuring technologies that were developed are directly applicable to other missile systems requiring cocured details such as Patriot vanes and LoAD structures.
- 3 The weight savings derived from the use of composite materials are significant and apply directly to any missile with trajectory limitations.
- 4 Labor and materials savings can be substantial by using composite air vanes.

Martin Marietta has five (5) recommendations for a follow-on program, which will be accomplished during the Option I program that is already under contract:

- Task 1 - Prepare the final version of the Implementation Plan.
- Task 2 - Reevaluate materials and mechanical properties with special emphasis on optimizing the prepreg material, compaction and cure cycle, molding pressure, and bonding materials, to reduce cycle times and to learn the effects of various molding pressures.
- Task 3 - Review structural and thermal analysis for the composite air vane and generate updated engineering drawings for all the components of the vane.
- Task 4 - Modify the compression mold and the bonding fixture for production use.
- Task 5 - Refine the manufacturing process to optimize the fabrication of the composite air vane with respect to mechanization and automation. Further, complete the NDI test procedure and validate the composite air vane for acceptance into the Pershing II Production Program.

To complete these recommendations will provide a composite air vane that can be implemented into production.



2.0 TECHNICAL DISCUSSION

The work accomplished during the program's basic effort comprised five major tasks:

- 1 Planning, including the initial implementation plan
- 2 Material and mechanical property evaluation
- 3 Design requirements and current vane redesign
- 4 Tool design and tool fabrication
- 5 Process demonstration and vane fabrication.

These tasks are interdependent as shown in Figure 2-1, and logically lead into Option 1. The task efforts were designed to develop the information required, both directly and with feedback, to successfully implement an efficient and cost effective composite air vane fabrication process.

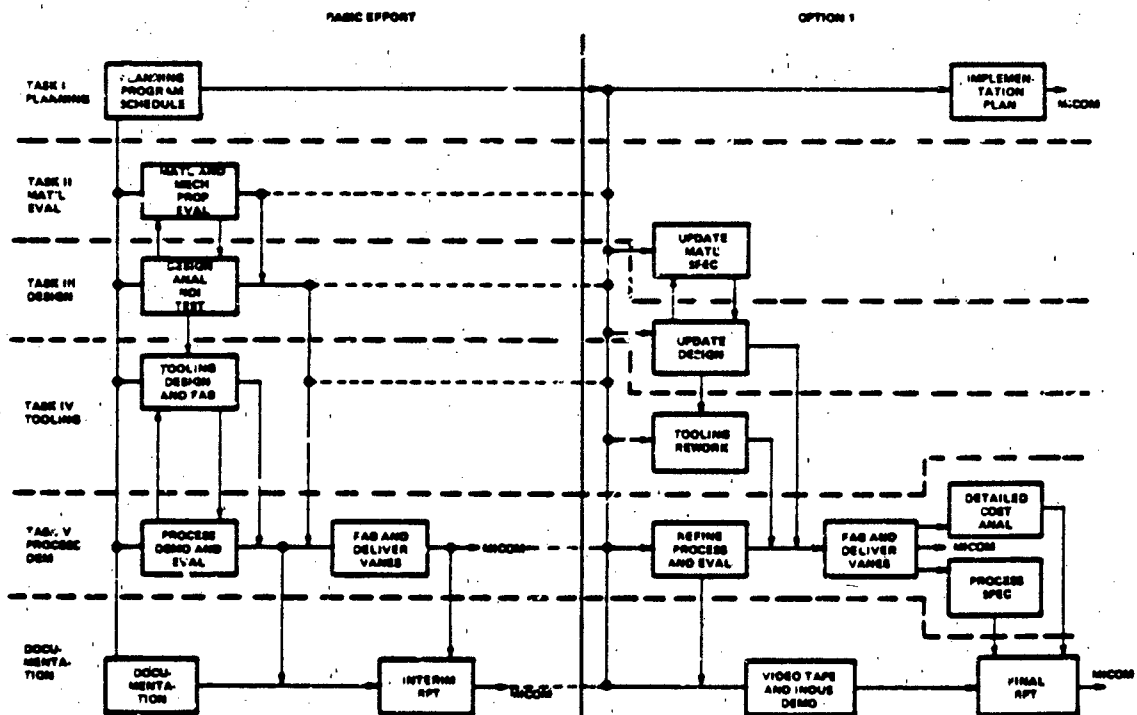


Figure 2-1. Major Tasks are Interdependent

The basic effort focused on the required materials and process selection, redesign of the Pershing II-type air vane (Ref. TR G0007) as a composite/Thermal Protection Structure, fabrication of the required tooling, establishment of processes to produce demonstration hardware, evaluation, and documentation. The basic effort activities were performed according to the program schedule in Figure 2-2 and are described below.



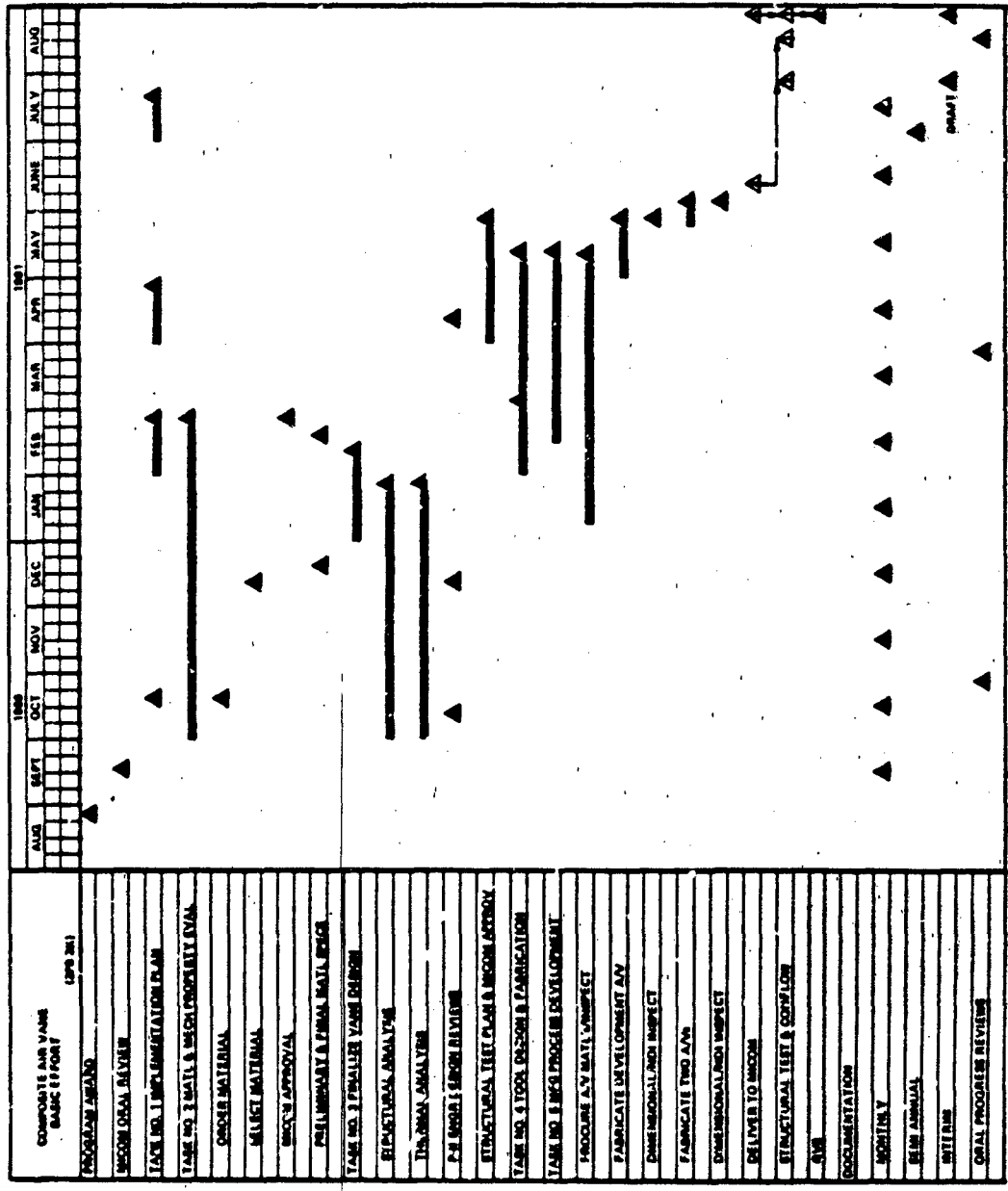


Figure 2-2. Composite Air Vane Basic Effort

2.1 Task I - Planning

Task I lead to the development of an implementation plan. The plan included: time to implement the program results into the composite air vane program, cost of implementation, identification of components to which the resulting technology would apply, a survey of potential applications outside Martin Marietta's facilities, and anticipated project benefits.

The first and most direct application of the technology resulting from this program would be to implement of the composite air vane into the Pershing II (Army) Program and into future Pershing missile programs. The technology gained during the span of the contract also could be applied directly to the Patriot (Army) missile vanes. The air vane design of the Patriot missile permits the use of composite materials in addition to curing technology that is also directly applicable. The weight savings created by the use of composite materials applies directly to any missile that has trajectory limitations. The fin or air vane can be transformed, with the technology gained from this program, into a composite structure that is lightweight and that will meet the structural requirements. U.S. military ship launched (Navy) cruise missiles that have air vanes would be candidates for this technology. Air Force Intercontinental Ballistic Missiles (ICBM) would greatly benefit from the composite air vane technology.

2.2 Task II - Material And Mechanical Property Evaluation

During the Material and Mechanical Property Evaluation study the graphite epoxy material, honeycomb, and adhesive were selected, and the mechanical properties of these materials were compared to the design criteria.

The manufacturing and design approach used for the low cost missile vane (Figure 2.2-1) provided a materials system intended to meet the structural and thermal requirements at the lowest manufacturing cost. A steel base structure with an integral shaft provided a rigid load path that was designed to resist shear, bending, and torsional loads. A composite skin with integral heat shield comprised the external contour. The internal volume consisted of a honeycomb core designed to transfer the transverse shear loads to the reaction points. These components are shown in Figure 2.2-2. The composite skin, acting as the primary load carrying structure, had significant impact on the overall strength of the air vane and was a major factor in the manufacturing cost.

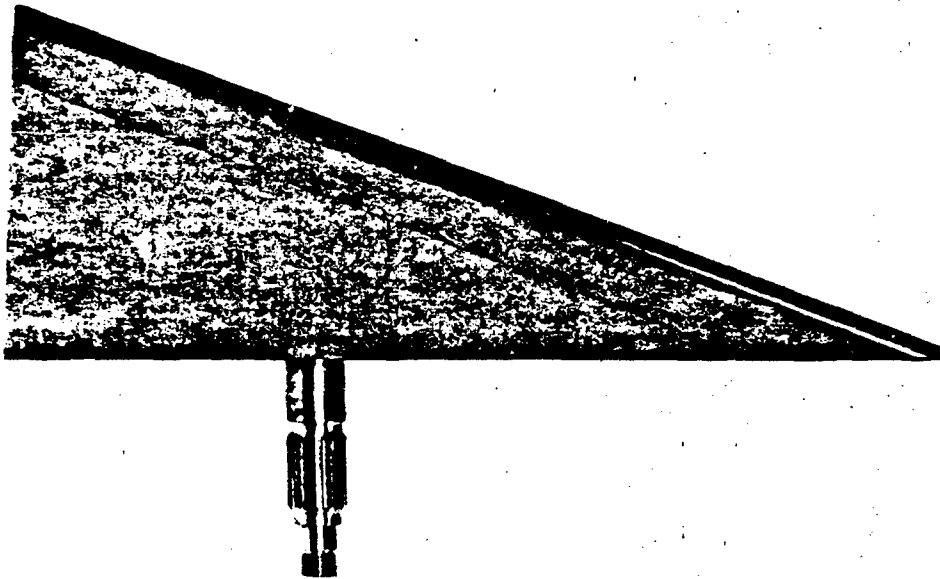


Figure 2.2-1. Low Cost Missile Vane

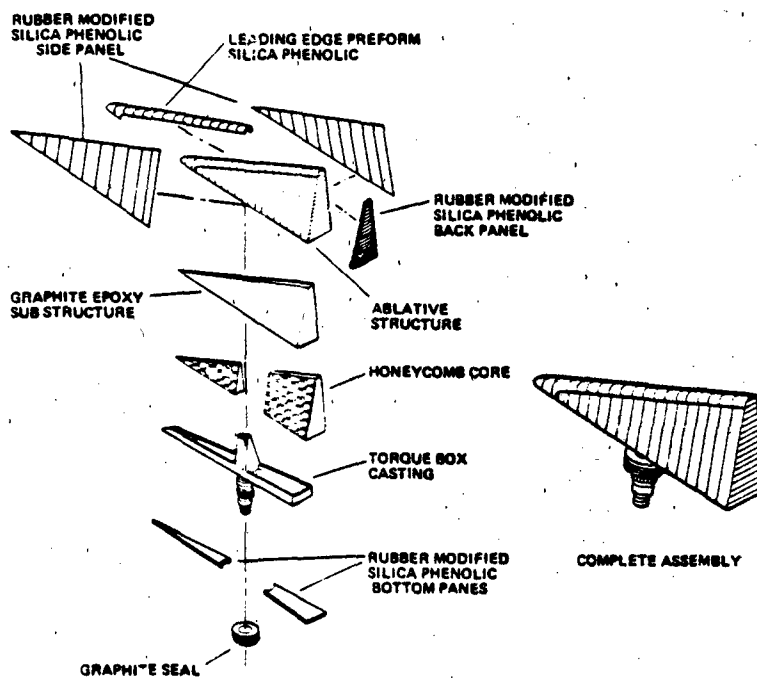
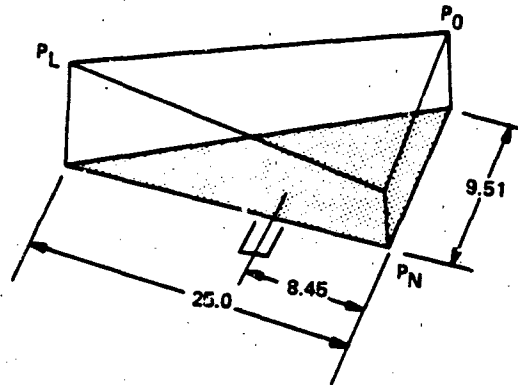


Figure 2.2-2. Low Cost Composite Air Vane Configuration

2.2.1 Composite Skin Requirements

Structural design requirements were identified in the early stages of Task III and are summarized in Figure 2.2.1-1.



Normal Force (lb)	Torque (in-lb)	Bending Moment (in-lb)	Max Tip Defl. (in)	Max Aft Defl. (in)	P_L (psi)	P_N (psi)	P_0 (psi)	Ult Factor
6800	5000	22600	0.35	0.16	72.2	68.4	30.2	1.25

Figure 2.2.1-1. Air Vane Structural Design Requirements

An improvement was apparent in the HT424 values, but the FM300 was still weaker than expected; the failure was in the adhesive, but no delamination occurred. Microscopic examination of the FM300 specimens that failed revealed minute air pockets in the fine-weave scrim cloth, reducing the cross-sectional area of the adhesive. Therefore, we decided to use HT424 in place of FM300 adhesive.

Two prime graphic epoxy candidate materials were selected and their properties are shown in Table 2.2.1-I.

Table 2.2.1-I

Graphite Epoxy Skin Material Candidates

Material	Form	Ply Thickness	Modulus (msi)		Tensile Strength (ksi)	
			E_x	E_y	F_x	F_y
<u>1</u> High Strength (T300/934)	Woven Fabric	0.013	10.6	9.6	80	80
<u>2</u> High Modulus (HMS/934)	Tape	0.007	26.5	1.3	53	4

The baseline 17-4PH metallic structure is shown in Figure 2.2.1-2. The calculations depicted in Table 2.2.1-I show that the lower cost T300 fiber meets the deflection requirements.

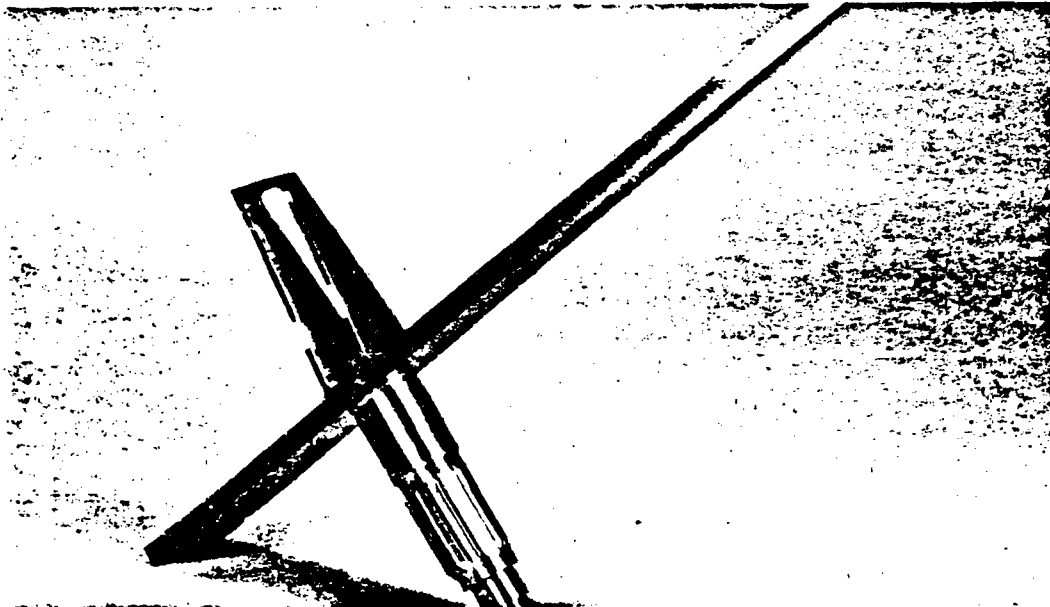


Figure 2.2.1-2. Air Vane Torque Box

Table 2.2.1-II

17-4PH Metallic Structure

Deflection Results

Skin Material	Orientation	Tip Deflection (in)	Aft Deflection (in)
<u>1</u> High Strength (fabric T300/934)	(090)(+45)	0.33	0.15
<u>2</u> High Modulus (tape HMS/934)	0/+45/90	0.28	0.13

Both materials met the design criteria. Therefore, because of lower cost, the high strength graphite epoxy T300/934 was chosen as the skin material.

A two-dimensional NASTRAN finite element model was used to evaluate the material candidates. The graphite epoxy skin/honeycomb combination was modeled as a flat plate with the equivalent bending stiffness. The root chord and shaft were represented as bar elements with the appropriate section material properties.

2.2.2 Adhesive and Honeycomb Core Evaluation

The air vane was designed to bond the cocured ablative/graphite epoxy structure to the steel frame and to the honeycomb core. Foaming adhesive HT424 (American Cyanamid) was selected to bond the honeycomb core to the frame. Film adhesive HT424 was chosen for bonding the remaining components. Fiberglass phenolic honeycomb comprised the core material. We tested several samples to verify the shear strength of the adhesive core interface, as cited in the following paragraphs.

2.2.2.1 Adhesive Testing

Adherends were cut into one inch square blocks by 0.30 inches thick. They were bonded together as shown in Figure 2.2.2.1-1 to make a compression double-lap shear specimen with one square inch of bond area. Different combinations were tested: all three blocks steel, all three graphite, and steel outside with a graphite center block. Film adhesives FM300 and HT424 were used on each combination. The steel used was 17-4PH stainless plate; the graphite was Fiberite T300 fiber/934 woven fabric (HMF 133/34).

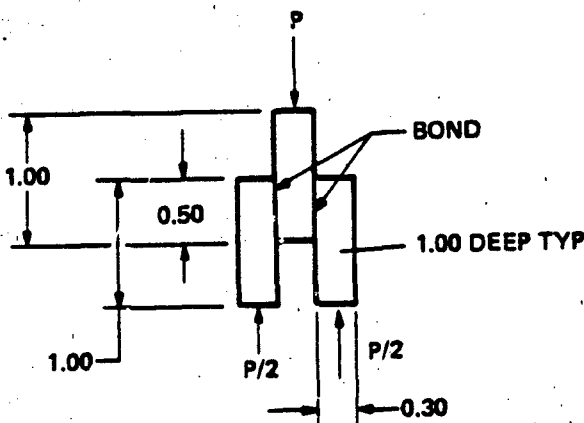


Figure 2.2.2.1-1. Double-Lap Shear Specimen Configuration

The specimens were loaded in compression by an Instron static test machine at room temperature, and maximum load and deflection were observed. The values for graphite specimens were lower than expected (See Table 2.2.2.1-I for reduced data on first set of specimens). Further, two all-graphite specimens had delaminations near one face. All failures were in the adhesive, plus the secondary delamination noted.

TABLE 2.2.2.1-I
First Adhesive Test

Adherends	Adhesive	No. of Specimens	Average failure shear stress, psi	Average deflection, in	Design ultimate stress, psi
All steel	FM300	3	6092	0.0054	6000
All steel	HT424	3	6560	0.0056	6000
All graphite	FM300	5	2758	0.0053	6000
All graphite	HT424	5	3034	0.0021	6000
Steel-graphite-steel	FM300	3	3125	0.0027	6000
Steel-graphite-steel	HT424	3	5083	0.0059	6000

A second set of all graphite and steel-graphite-steel specimens were made, then trued flat and square by a light machining pass after the bonding operation. Test results are shown in Table 2.2.2.1-II.

TABLE 2.2.2.1-II
Second Adhesives Test

Adherends	Adhesive	No. of Specimens	Average failure shear stress, psi	Average deflection, in	Design ultimate stress, psi
All graphite	FM300	5	3052	0.0048	6000
All graphite	HT424	5	6556	0.0084	6000
Steel-graphite-steel	FM300	3	3739	0.0050	6000
Steel-graphite-steel	HT424	3	6737	0.0070	6000

An improvement was apparent in the HT424 values, but the FM300 was still weaker than expected; the failure was in the adhesive, but no delamination occurred. Microscopic examination of the FM300 specimens that failed revealed minute air pockets in the fine-weave scrim cloth, reducing the cross-sectional area of the adhesive. Therefore, we decided to use HT424 in place of FM300 adhesive.

2.2.2.2 Honeycomb Core Test

The fiberglass/phenolic cores (3/16-in. hexagonal cell, 5.5 lb. per cubic foot) were tested in two loading configurations (see Figure 2.2.2.2-1). In the first configuration the faces of the cells were bonded to the load plates and the load was applied perpendicularly to the cell direction. In the second configuration, the edges of the cells were bonded and the load was applied parallel to the cell direction.

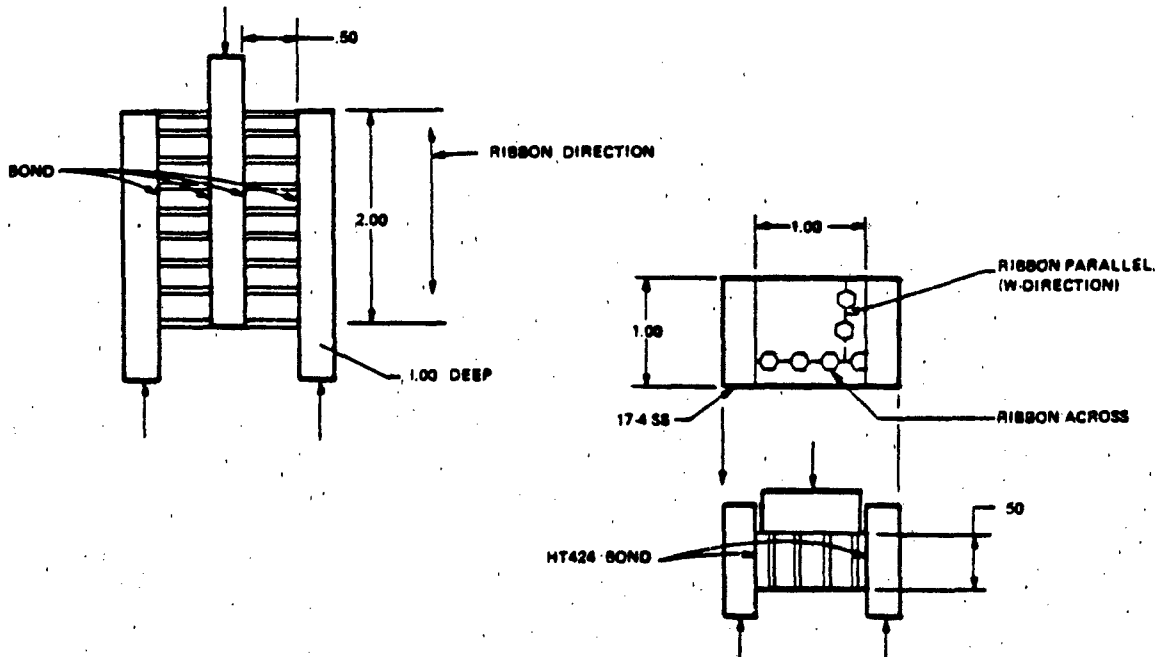


Figure 2.2.2.2-1: Honeycomb Specimen Configuration

In the first configuration, graphite/epoxy adherends similar to the adhesive test were used, along with both FM300 and HT424 adhesives. The core's ribbon direction was vertical, i.e., loaded in the test. The adhesive was cured at 40 psi and 340°F.

In the second configuration, 17-4PH stainless steel adherends were used, and only HT424 adhesive was applied. Two sets were made, one with the ribbon direction of the core across the adherends, the other with the ribbon parallel to the adherends. Note that film adhesive was used instead of the foaming type called for in the vane design. Foaming would stiffen the cell walls on the edge and would be as strong or stronger than the film type. Also, light pressure (5 psi) was applied to clamp the parts during cure since the core deforms easily.

Specimens were loaded in compression in an Instron static test machine at room temperature, and failure loads and deflections were observed. The specimens loaded along the cell direction had the load applied by a steel plate loosely fitted between the adherends to avoid resting it on the adhesive fillets.

As shown in Table 2.2.2.2-I, all specimens failed by shearing the core. The comparison data were supplied by Hexcel, Inc., manufacturer of the core.

TABLE 2.2.2.2-I
Honeycomb Core Shear Tests

Load Direction	Adhesive	No. of Specimens	Average failure shear stress, psi	Average deflection, in	Minimum design shear strength
Perpendicular to cells	FM300	5	403	0.0286	370
Perpendicular to cells	HT424	5	381	0.0253	370
Parallel to cells, ribbon direction	HT424	4	417	0.0183	370
Parallel to cells, "W" direction	HT424	4	332	0.0128	190

2.3 Task III - Design

Task III involved performing a structural and thermal analysis and developing a structural test plan.

2.3.1 Structural Analysis

A three-dimensional finite element structural model was developed using NASTRAN computer code. Each of the structural elements was represented by an appropriate finite element model which was illustrated by the computer graphics program, Supertab. The overall model was established by superimposing the structural elements. The finite element models are shown in Figures 2.3.1-1, 2.3.1-2 and 2.3.1-3 and are described in the following paragraphs. Table 2.3.1-I shows material properties input and Table 2.3.1-II depicts the honeycomb properties.

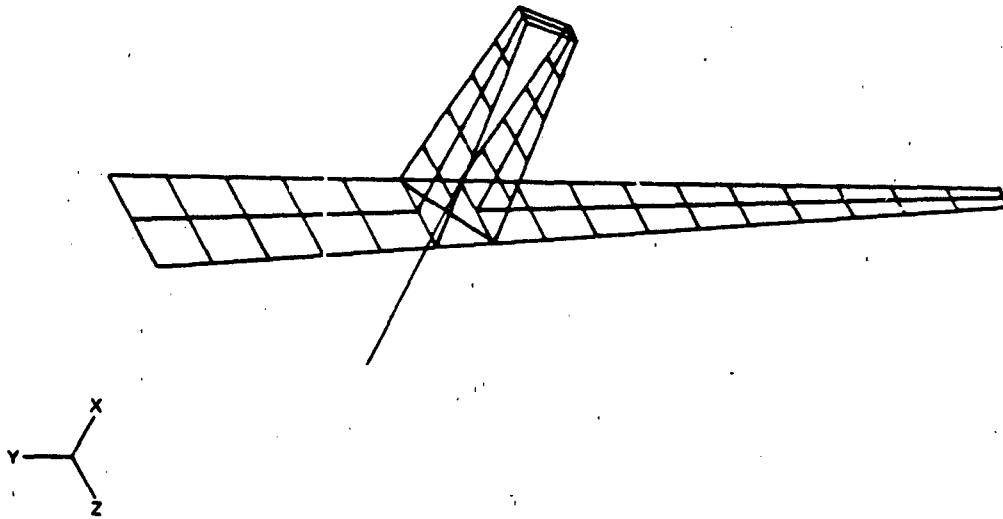


Figure 2.3.1-1. Finite Element Analysis - Steel Base

Table 2.3.1-I
Material Properties Input

	GRAPHITE	HEAT SHIELD	GRAPHITE/H.S.
E _x (10 ⁶ psi)	7.09	2.1	3.61
E _y (10 ⁶ psi)	7.09	1.2	3.01
ν _x	0.332	0.25	0.31
G _{yy} (10 ⁶ psi)	2.66	0.8	1.36

Table 2.3.1-II
Honeycomb Properties

	THICKNESS (inches)	E 10 ⁶ psi	G 10 ⁶ psi	
Ribbon Direction	0.018	3.0	1.2	0.25
Transverse Direction	0.009	3.0	1.2	0.25

Stainless Steel Base

The steel base (Figure 2.3.1-1) of the air vane was channel shaped and was modeled using plate elements along the bottom of the channel. Beam elements were used to model the sides of the channel. This type of representation accurately describes the changing cross sections seen in the base. Beam elements were also used to model the shaft. Beam elements typically have stiffness axially, in bending, torsion, and shear. The torque bars were modeled with plate elements. Plate elements have stiffness in the same manner as the beam element in this configuration. The outboard bearing supports the shaft in the Y and Z directions. The second bearing supports the shaft in the X, Y, Z, and rotation about the X direction.

The shell was modeled using rectangular and triangular plate elements. This type of configuration was advantageous since material properties could be readily changed. One analysis was performed using just the graphite shell. In another analysis, the resultant properties of the graphite/heat shield combination were entered. The resultant properties of the graphite/heat shield combination were obtained from the Point Stress Laminate Analysis computer program SQ5. Also note that the orientation of the plate elements coincide with the laminate axis system.

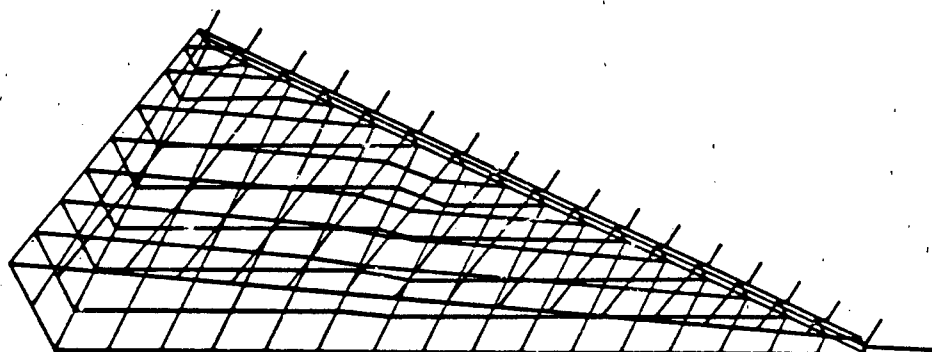


Figure 2.3.1-2. Finite Element Analysis - Shell

The leading edge was modeled as a beam element with graphite properties. To obtain deflections at the tip of the leading edge, beam elements were extended to those points. Deflection is shown in Table 2.3.1-III.

Table 3.2.1-III

Air Vane Deflection Under Maximum Load Condition

LOCATIONS (See Figure 2.3.1-4)	DEFLECTION, INCHES	
	ANALYSIS	MAXIMUM ALLOWED
L	0.206	0.35
O	0.145	0.16
P	0.011	0.05

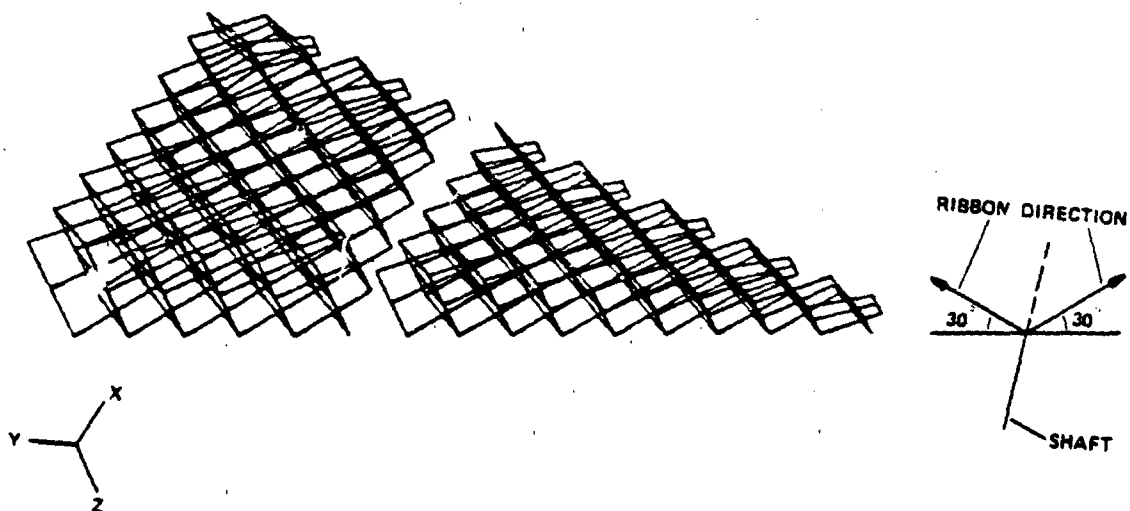
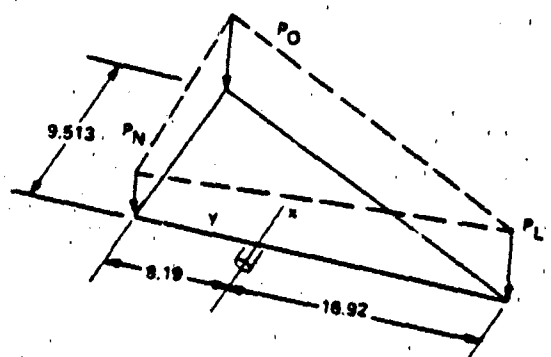


Figure 2.3.1-3. Finite Element Analysis - Honeycomb Core

The honeycomb was represented by a square matrix of plate elements. The plates were only given shear stiffness to represent the actual honeycomb. The ribbon direction of the honeycomb was oriented such that the strongest part of the honeycomb directed the load toward the base of the shaft (a 30 degree angle). A square configuration may be used to model the honeycomb since honeycomb properties may be considered bi-directional.

Analysis Results

Two loading conditions were analyzed as given in Figure 2.3.1-4. The loads normal to the vane mid-plane were applied to the grid points of the upper shell surface in accordance with the pressure distribution corresponding to each of the conditions.



COND 1 - MAX LOAD - $P_L = 72.2$ psi; $P_N = 30.2$ psi; $P_O = 68.4$ psi
 $V = 6800$ LBS; $M_y = 22800$ IN-LBS; $M_x = 5040$ IN-LBS

COND 2 - MAX TORQUE - $P_L = 58.9$ psi; $P_N = 1.7$ psi; $P_O = 29.3$ psi
 $V = 3500$ LBS; $M_y = 8484$ IN-LBS; $M_x = 7500$ IN-LBS

Figure 2.3.1-4. Air Vane Structural Design Requirements

The results from the NASTRAN finite element analysis show that the critical stresses and deformations occur under the maximum load condition. Therefore, only the results from that loading condition are reported. The structural configuration corresponds to the one without the external heat shield.

The maximum stress in the graphite/epoxy skin occurs in an element forward of the steel torque box and next to the root rib. The limit stress is 12,800 psi.

$$\text{Ultimate Margin of Safety (M.S.ULT)} = \frac{65,000}{1.25 (12,800)} - 1 = +3.06$$

The maximum shear stress in the glass/phenolic honeycomb core occurs in the area just forward of the torque box located at one third the span of the torque box. The limit shear stress is 280 psi.

$$\text{Ultimate Margin of Safety (MSULT)} = \frac{370}{1.25 (280)} - 1 = +0.06$$

2.3.2 Thermal Analysis

The thermal design trajectory used for heat shield sizing was based on a 3 σ (hot) motor performance for both the first and second stage motors (highest possible velocity during ascent). Maximum heatflux during this portion of flight was less than 30 BTU/ft²-s. The exoatmospheric coast period does not cause any additional heatflux, but because of its long duration, the heat received during ascent is absorbed down to the substructure. Therefore, the bulk temperature of the heat shield and structure is 210°F by the start of reentry.

The air vane leading edge (bottom pair of vanes) was exposed to very high heating due to near stagnation local pressures during the initial pull-up portion of reentry (as shown in Figure 2.3.2-1). This magnitude of local pressure (about 17 atmospheres) caused the cold wall heatflux to reach a peak of greater than 4000 BTU/ft²-s (Figure 2.3.2-2). The predicted thermal recession of the silica phenolic (0.50 inch radius) was approximately 0.22 inch. The rain field, which the RV was expected to be able to fly through, was contained in the final portion of the flight (from 38,000 feet to the ground) at the time when the heat shield material had experienced maximum charring. The predicted maximum rain erosion was approximately 0.35 inch, and adding this value to the thermal recession yielded a total recession of 0.57 inch.

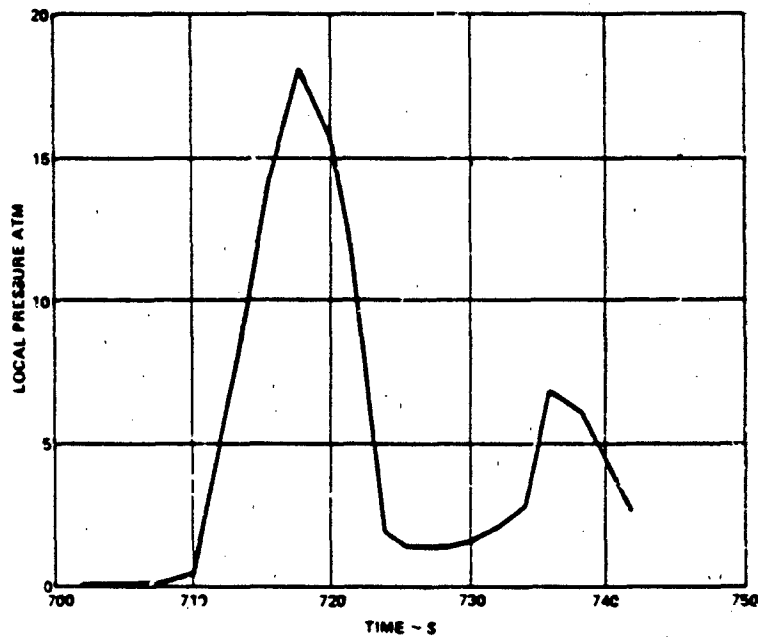


Figure 2.3.2-1. RV Fin Leading Edge Local Pressure During Reentry

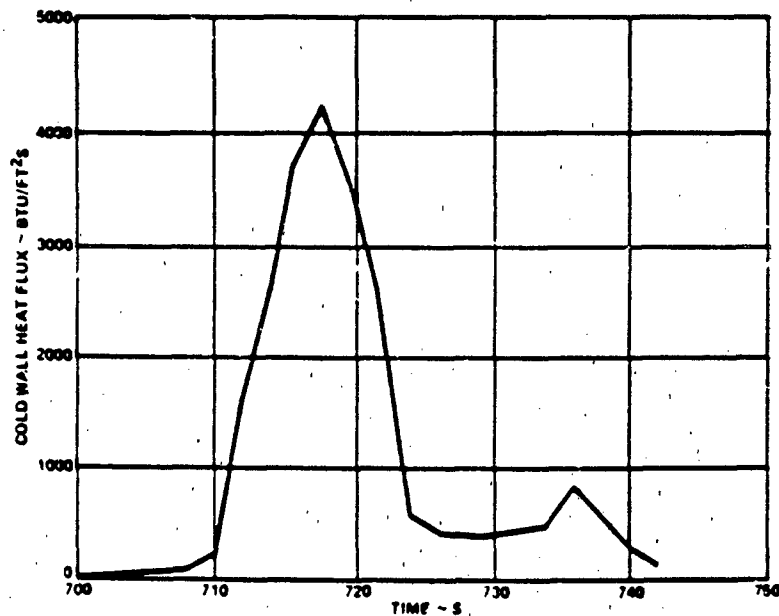


Figure 2.3.2-2. RV Fin Leading Edge Cold Wall Heat Flux During Reentry

The heat flux (Figure 2.3.2-3) on the RV vane side panels (lower pair of vanes) was significantly lower than on the leading edge, and only slightly greater than that on the RV body at this location. The increase in heating over that which occurred on the body was due to the increased surface angle, (raper angle 7 degrees as opposed to 3.3 degrees body angle), and also due to vane deflections for vehicle control during reentry.

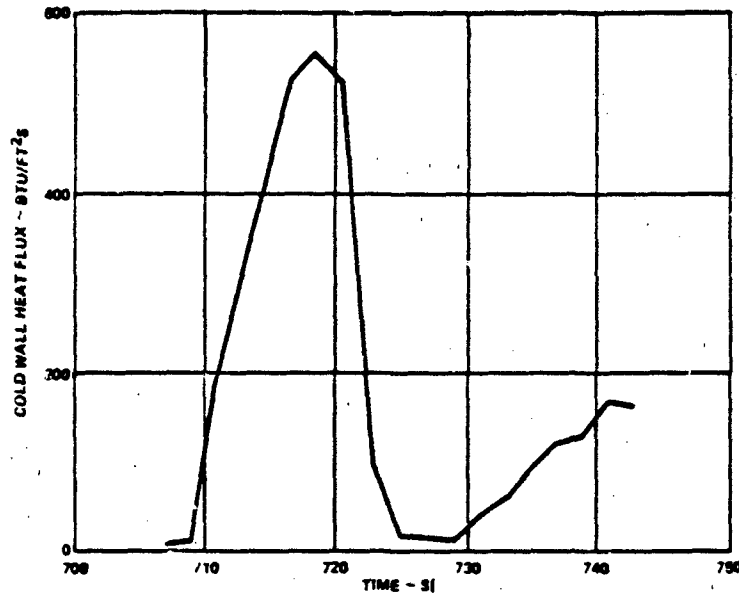


Figure 2.3.2-3. RV Fin Side Panel Cold Wall Heat Flux During Reentry

The root chord panel was another area of concentrated heating, since heat augmentation occurred due to the gap between the vane bottom side and RV body (vane pad), particularly in the area just ahead of the vane shaft. The resulting heat flux was estimated to be approximately 3.4 times higher than the (unaugmented) body heat flux as shown in Figure 2.3.2-4. Because of the high level of augmented heating in this area, it was recommended that the root chord substructure (stainless steel) contain no lightening holes forward of the vane shaft; we believe that the solid structure is necessary for use as a heat sink. Previous experience on the SAM-D (Patriot) program has shown that vane failure will occur due to heat shield burn through at lightening hole locations ahead of the shaft.

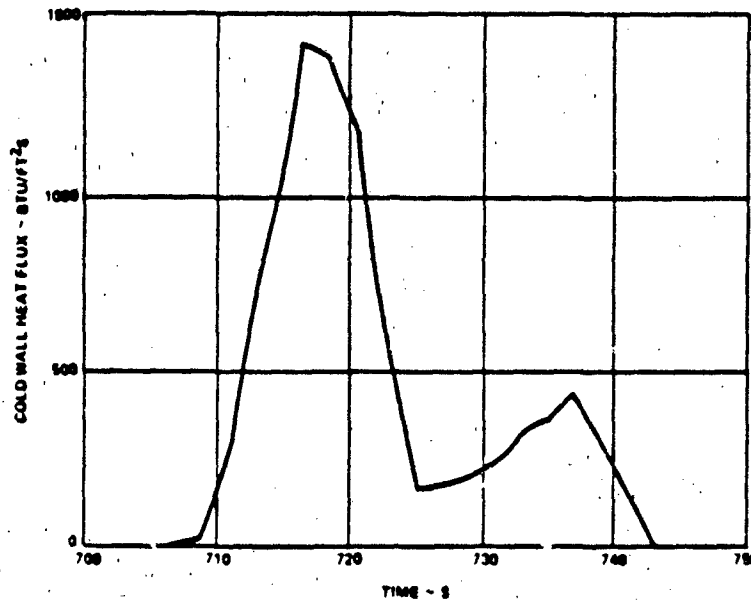


Figure 2.3.2-4. RV Fin Bottom Gap Augmented Cold Wall Flux During Reentry

The composite air vane was analyzed thermally to define the thickness necessary for the ablative materials - silica phenolic and rubber modified silica phenolic. The complete analysis is detailed in Appendix A. In summary, we found that the side panels would require a minimum of 0.240 inches of ablative, the root chord 0.218 inches, and the trailing edge 0.217 inches (see Table 2.3.2-I). The current PII reentry thermal design trajectory plus worst case assumptions and rain erosion were considered in this analysis.

TABLE 2.3.2-I
Composite Airvane Heatshielded Sizing Summary

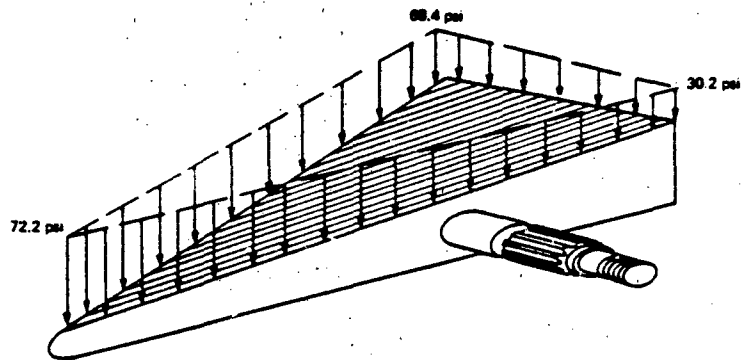
Vane Section	Leading Edge	Side Panel	Root Chord	Trailing
Substructure Thickness (in)	Graphite Epoxy/0.10	Graphite Epoxy/0.10	Stainless Steel/0.10	Graphite Epoxy/0.10
Heatshield Material	Silica Phenolic	RMSF	RMSF	RMSF
Thickness Required Due to:				
Thermal Recession (in)	0.220	0.007	0.089	<0.001
Rain Erosion (in)	0.350	0.146	N/A	N/A
Bondline/Substructure (in) (Max Temp, °F)	0.030 (350)	0.87 (350)	0.129 (600)	0.217 (350)
Minimum Thickness ¹ (in)	0.600 ²	0.240	0.218	0.217

Notes: 1) All heatshield thicknesses shown above are minimum. Nominal tolerance for heatshield layup is ± 0.010 -inch.

2) Radius is 0.50-inch.

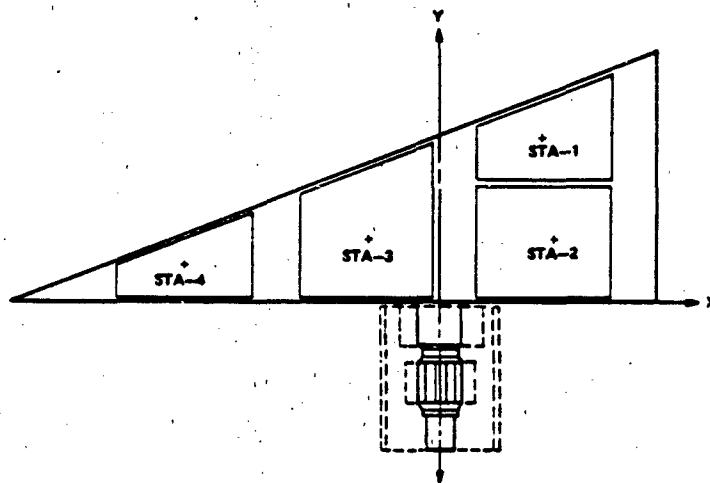
2.3.3 Static Test Plan

A static test plan was developed to verify the structural integrity of the composite air vane. The test was accomplished by mounting the air vane in a test fixture and applying loads until vane failure (or a maximum load of 200 percent DLL) occurred. Load, strain, and deflection data were recorded. A support fixture held the air vane in a manner simulating a missile installation, which allowed the proper shear, bending moment, and torsion reactions to the vane shaft. Sponge rubber pads backed up by steel plates provided a distribution of test loads based on operating air loads (Figures 2.3.3-1 and 2.3.3-2). Aluminum bars spanned the air vane and bore on the steel pads at locations where test loads were applied. A system of levers and turnbuckles (whiffletree) branched the various point loads into a single test load (Figure 2.3.3-3), while a 20,000 pound capacity hydraulic actuator and a 20,000 pound electronic load cell made up the remainder of the load line. A hydraulic hand pump pressurized the actuator.



DESIGN LIMIT LOAD	
Total Normal Force	6 800 pounds
Torque	5,040 in-lb
Bending Movement	22,599 in-lb
Max Tip Deflection	0.35 inch
Max Aft Deflection	0.16 inch

Figure 2.3.3-1. RV Design Limit Load



STATION	TEST LOAD (LBS)	LOCATION (IN)		TORQUE IN LB	MOMENT IN LB
		X	Y		
1	1595	4.34	6.61	6922	10,543
2	1865	4.34	2.72	8094	5,073
3	1800	-2.86	2.73	-5148	4,914
4	1540	-9.67	1.34	-14,892	2,064
TOTAL	6800			-5,024	22,594

Figure 2.3.3-2. Composite Air Vane Test Load Distribution.

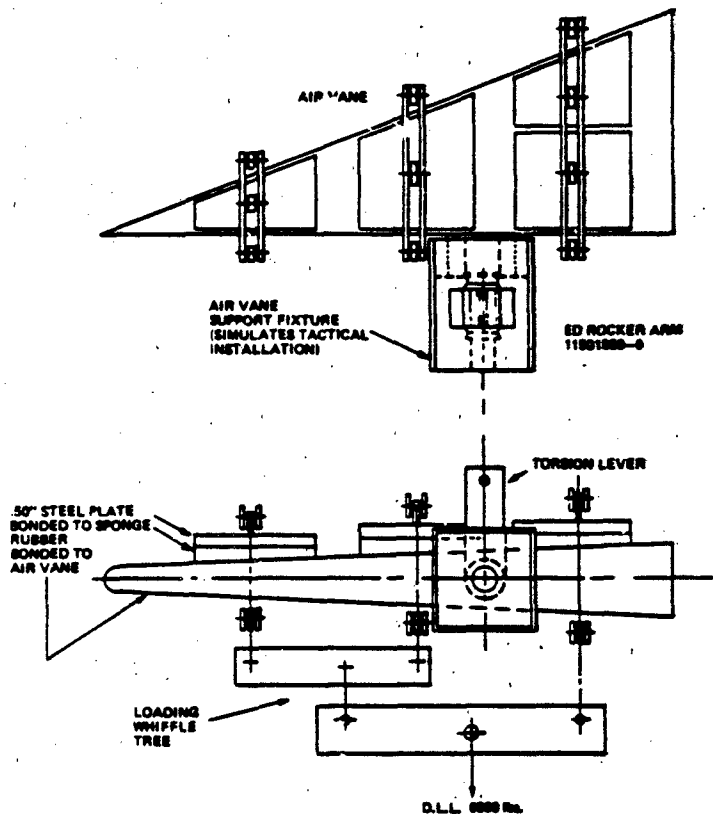


Figure 2.3.3-3. Static Test Fixture Load Arrangement

An automatic data acquisition system (a multi-channel system using a magnetic tape recorder) recorded and processed load, strain, and deflection data. It also provided signal conditioning, zero and balance circuitry, "quick look" or visual readout on limited selected channels, printout, and acquired data plotting. All measuring instruments had current calibrations traceable to the National Bureau of Standards.

A BLH dual channel electronic load cell measured the test load. One channel was for visual indication, used during the loading procedure; the second channel was for data acquisition.

DC Displacement Transducers (DCDT) (Figure 2.3.3-4) measured displacement, normal to the mid planform plane, at five locations on the air vane. The rosette strain gages were attached to the air vane as shown in Figure 2.3.3-5.

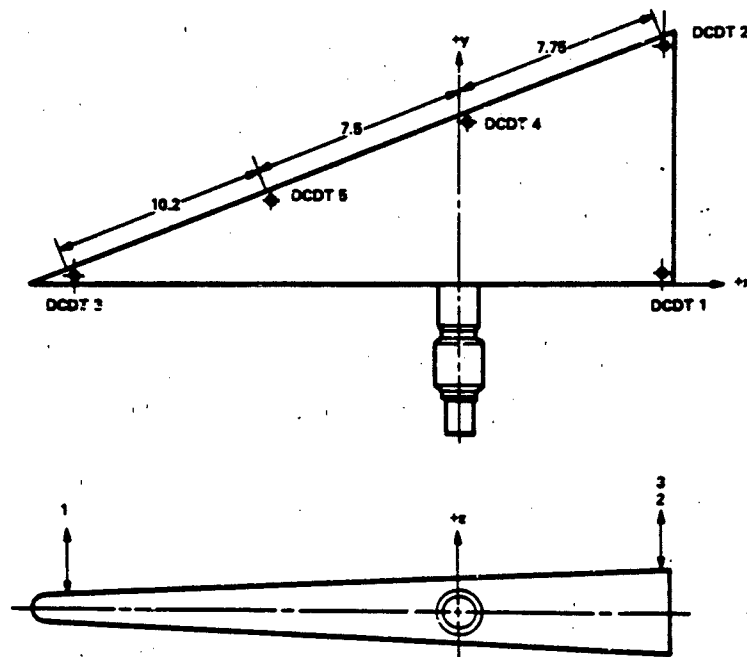


Figure 2.3.3-4. Location of Deflection Measurements

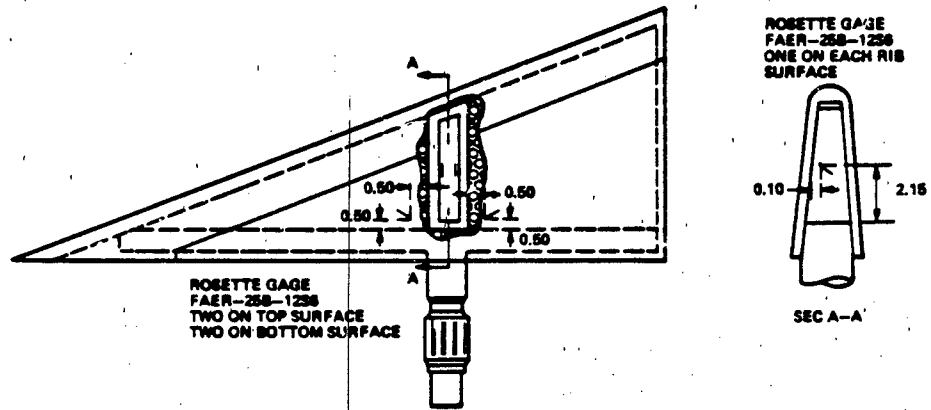


Figure 2.3.3-5. Location of Rosette Strain Gages

The test consisted of the following procedures:

- 1 Perform a pretest visual inspection of the air vane and record observations in the test log.
- 2 Install strain gages.
- 3 Install the air vane in the support fixture.
- 4 Mount the air vane support fixture assembly to the base structure.
- 5 Attach the loading apparatus.
- 6 Install deflection gages.
- 7 Record the identity in the test log (manufacturer, model number, EQ number), calibration due date, and location of all measuring instruments.
- 8 Photograph the test setup. (Figure 2.3.3-6).
- 9 Complete electrical hookup of all instrumentation.
- 10 Balance and obtain zero readings of load, strain, and deflection readings.
- 11 Apply 350 to 400 pound loads to check out all systems.
- 12 Remove all load; rebalance and zero as necessary.

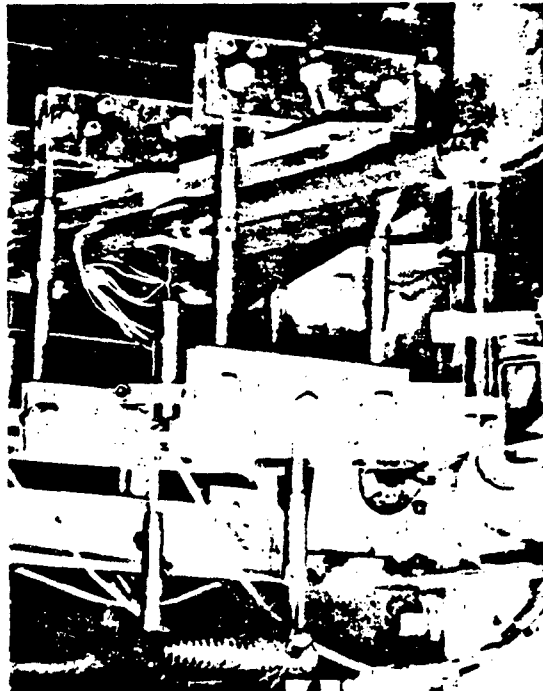


Figure 2.3.3-6. Static Test Article in Test Fixture

- 13 Apply the load profile in Table 2.3.3-I at a slow and steady rate (30 seconds minimum between increments). Hold the load at each increment approximately 1 minute.
- 14 Remove test article from test setup.
- 15 Perform visual inspection and record observations in test log.
- 16 Photograph failed parts (if applicable).
- 17 Teardown test setup.
- 18 Replay data tabulation and perform data plots as directed by test engineer.
- 19 Shutdown and secure data acquisition system. Record magnetic tape file number in test log.

Table 2.3.3-I
Static Test Loading Profile

LOAD INCREMENT (% DLL)	TOTAL LOAD (POUNDS)	20K LOAD CELL READING
0	0	0
20	1360	6.8
40	2720	13.6
60	4080	20.4
80	5440	27.2
20	1360	6.8
80	5440	27.2
100	6800	34.0
*120	8160	40.8
140	9520	47.6
160	10,380	54.4
180	12,240	61.2
200	13,600	68.0
0	0	0

*If failure has not occurred, remove DCDT instruments after 120 percent DLL load.

2.4 Task IV - Tool Design And Fabrication

Manufacturing Research and Technology and Engineering Prototype Laboratory personnel performed the tool design, while LB Engineering, Inc., carried out tool fabrication. The types of tools listed below were fabricated during the basic effort and will require minor modifications for use in the Option I program:

- 1 Matched metal die compression mold for net molding of cocured structure (see Figure 2.4-1).



Figure 2.4-1. Matched Metal Die Compression Mold for Net Molding of Cocured Structure

- 2 Matched metal bonding adapter plate for bonding of cocured structure to honeycomb torque box assembly (see Figure 2.4-2).

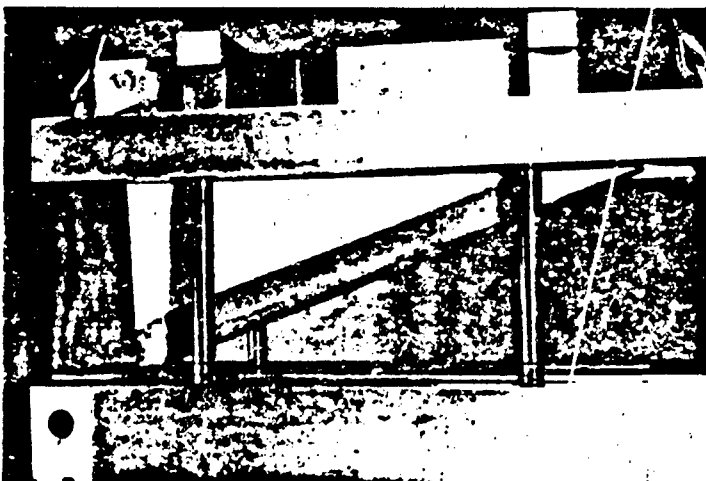
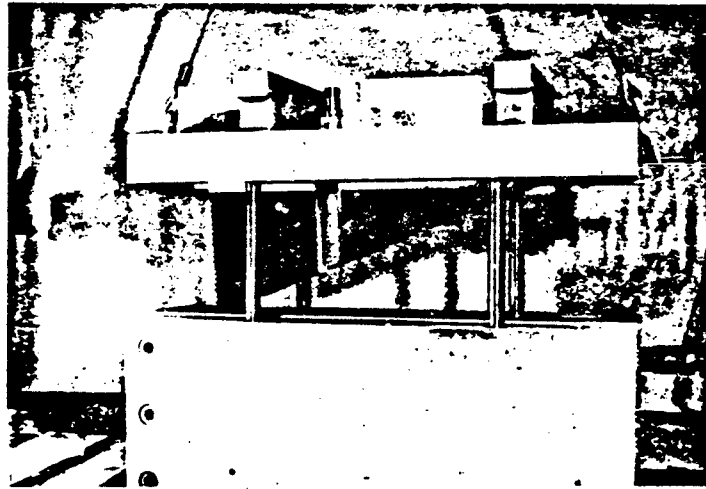


Figure 2.4-2. Matched Metal Die Bonding Assembly for Bonding Honeycomb Torque Box Assembly to Cocured Structure

- 3 Graphite epoxy substructure on staging tool and templates (see Figure 2.4-3).

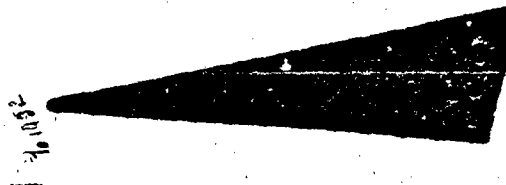


Figure 2.4-3. Graphite Epoxy Substructure Staging Tool and Template

- 4 Ablative side panel, back panel, and bottom panel templates (see Figure 2.4-4).

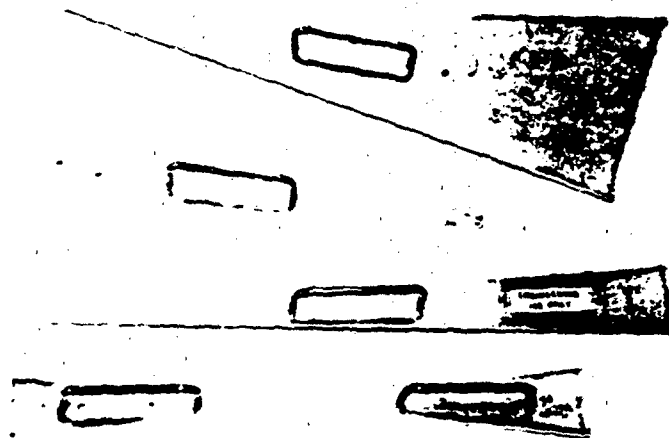


Figure 2.4-4. Ablative Side Panels, Back Panel and Bottom Panel Template

- 5 Leading edge folding wedge and staging tool (see Figure 2.4-5).

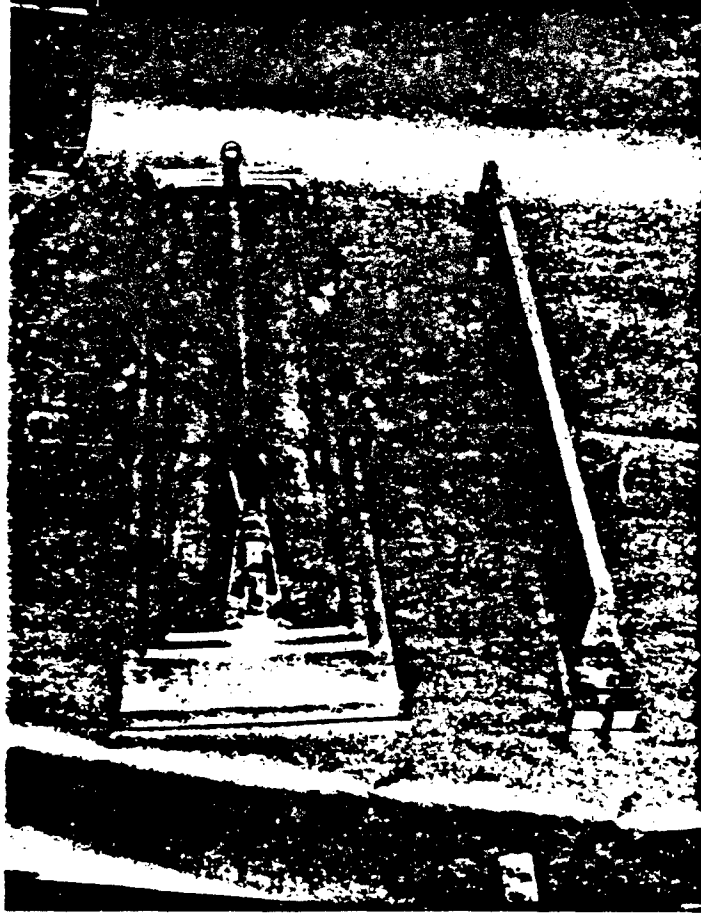


Figure 2.4-5. Leading Edge Folding Wedge and Staging Tool

2.5 Task V - Process Demonstration

During the process demonstration task Martin Marietta Orlando Aerospace manufactured seven composite air vanes, two of which underwent static testing.

2.5.1 Fabrication

The following explains in detail the approach used for fabricating the composite air vanes.

Metallic Substructure

In full scale production the metal substructure will be procured as a 17-4PH stainless steel casting. The structure shown in Figure 2.2.1-2 was machined from 17-4PH plate stock. Final machining of the close tolerance shaft diameter and concentric bearing grooves was accomplished on an N/C lathe.

Ablative Heat Shield Side, Bottom, and Back Panels

Wrapping the acrylonitrile butadiene silica phenolic tape was accomplished on a high speed, horizontal semiautomatic tape wrap machine (Figure 2.5.1-1), which wrapped the three-quarter inch wide bias tape on a mandrel at a 30-degree shingle angle. Bias tape was used for shingle wrapping because it will distort to conform to the mandrel surface; however, the controlled distortion is a function of the specific wrap geometry. Due to the difference in circumference, the tape edge in contact with the mandrel surface is fed more slowly than the outer edge of the tape. This difference in surface speed induces tape distortion by forcing the weave pattern of the tape to stretch across its width, and maximum distortion occurs at the outer edge. Maximum distortion is a function of the ratio of mandrel surface tape circumference to outer tape edge circumference. Tape wrapping without wrinkles became easier as the ratio approached one. Ratios larger than one made successful bias wrapping difficult.

The wrapped mandrel was removed and mounted on a lathe. The OD of the rubber modified silica phenolic was turned to a predetermined thickness and cut horizontally along the mandrel, thus controlling wall thickness and reducing shingle angle distortion during net molding. The phenolic preform was removed from the mandrel and flattened. Individual preforms for the side, bottom, and back heat shield were rough sawn and hand sanded to actual size. Each preform was sealed and placed in cold storage.

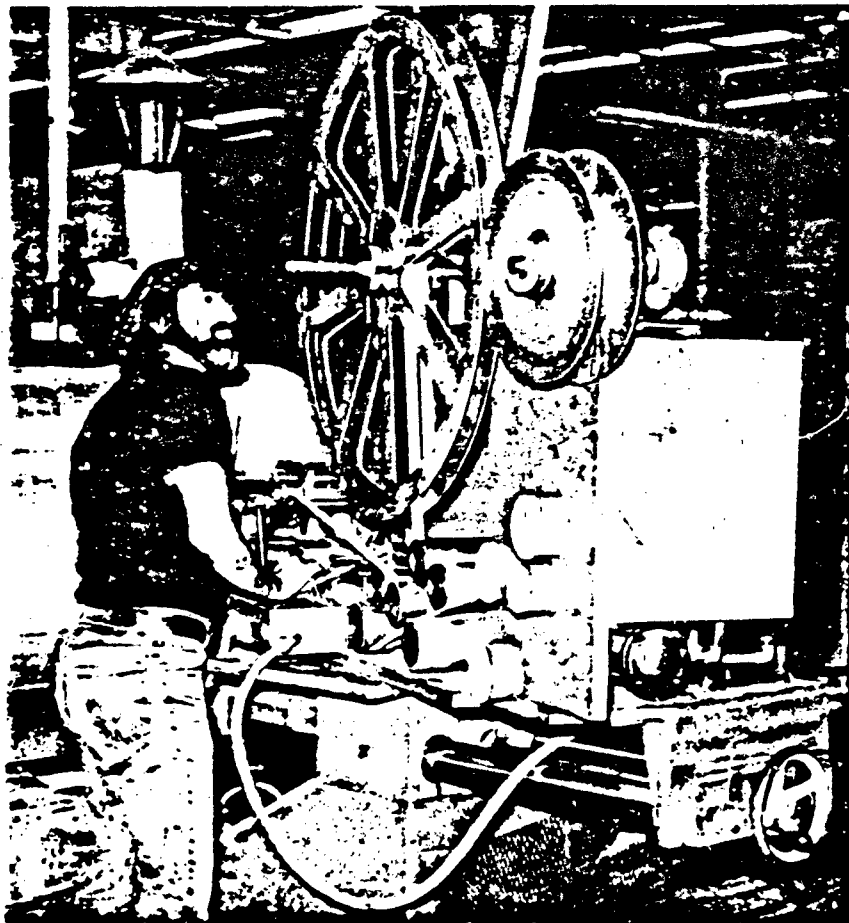


Figure 2.5.1-1. Tapewrapping of Ablative Heatsheild for Side, Bottom and Back Panels

Silica Phenolic Leading Edge

The leading edge (Figure 2.5.1-2) was fabricated from two-inch wide bias tape. After the tape was cut into the required number of pieces and to the proper length, an approximate 30-degree shingle angle laminate was layed up on a preform mold, vacuum bagged, and staged in an oven for 30 minutes at 180°F. After inspection of the shingle angle, staging time and temperature, debulk thickness, and miniature flow percent, the preform was saw cut to shape and face milled. The preform was then machined to form the 0.5 inch L/E radius and the preform legs were machined to proper thickness.

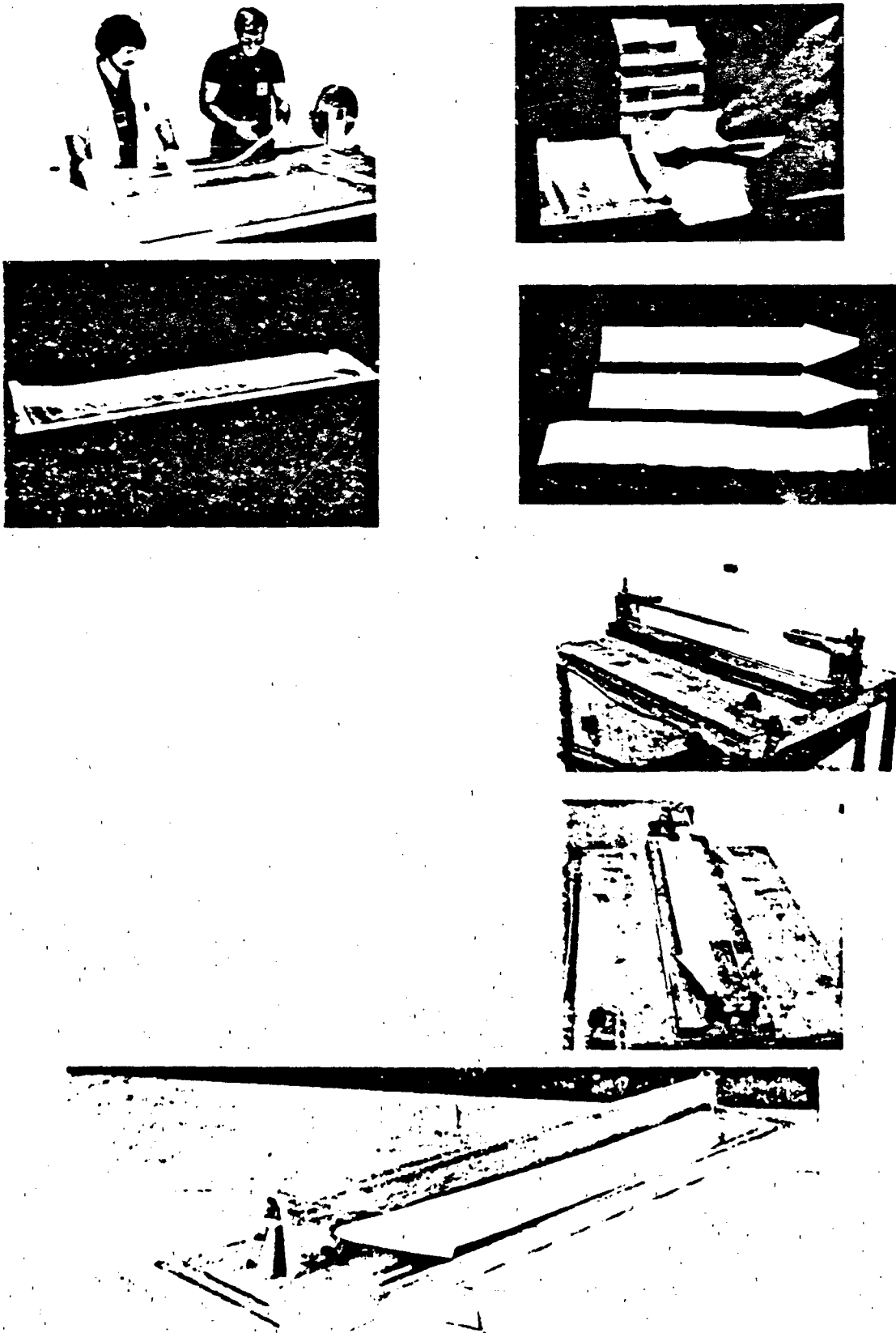


Figure 2.4.1-2. Silica Phenolic Leading Edge Fabrication Process

The leading edge preform was placed on a caul plate and heated to 180°F. It was then folded (Figure 2.5.1-3) on a modified Pershing II ED folding fixture. The folded preform was placed on a preform tool and staged, as required, under vacuum to even out the preform legs and to complete the staging operation.

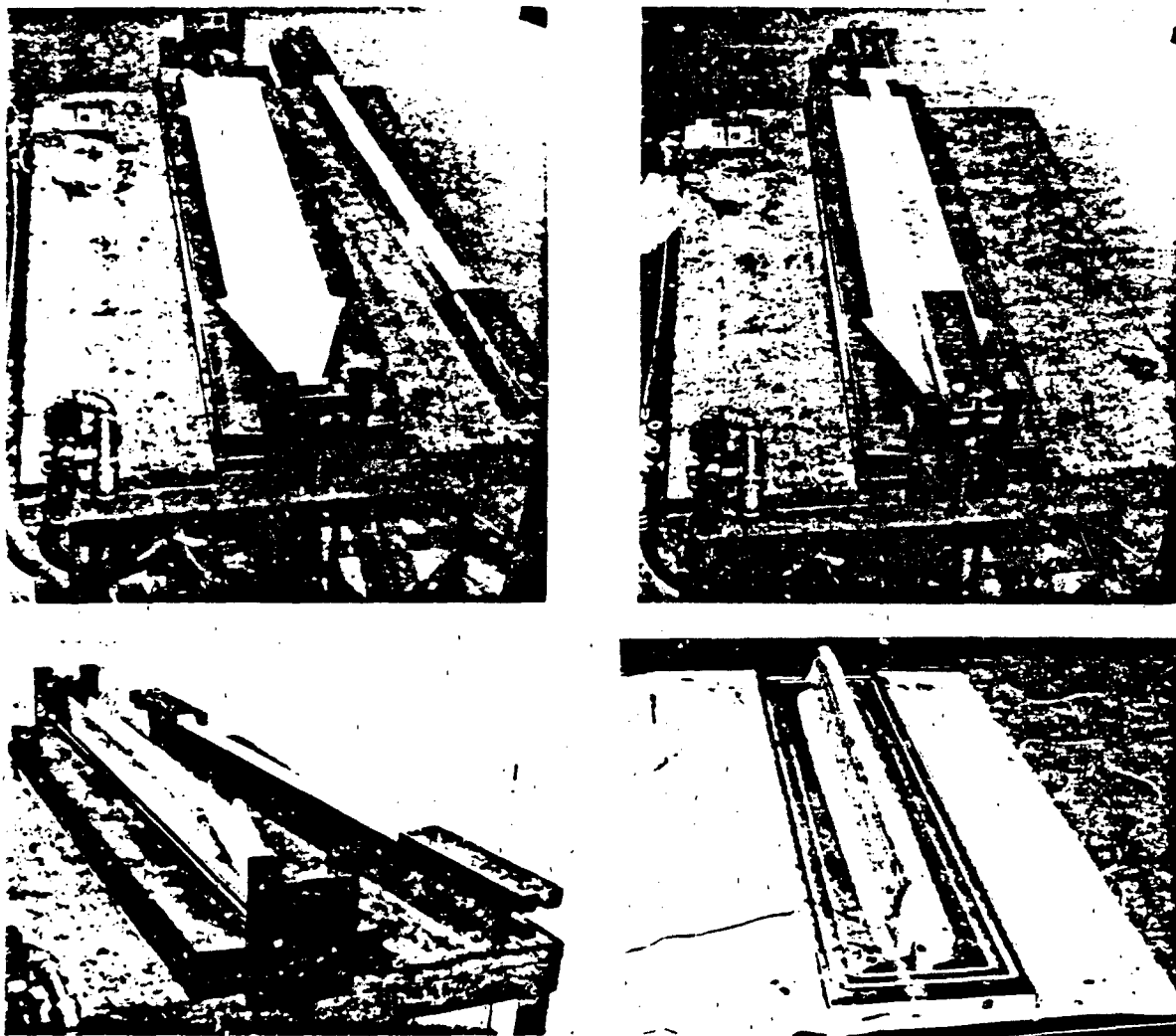


Figure 2.5.1-3. Folding Leading Edge Preform and final Staging

Graphite Substructure

Plies of graphite epoxy broadgoods were cut to patterns with the proper orientation. The flat pattern layups were positioned on the aluminum staging tool and densified at 180°F for 30 minutes (see Figure 2.5.1-4).



CUTTING OF GRAPHITE EPOXY



STAGING TOOL & TEMPLATES

Figure 2.5.1-4. Graphite Epoxy Substructure Lay Up

Composite Net Molding

During the coating of the compression mold with mold release, two rubber modified silica phenolic heat shield panels, a graphite epoxy substructure, and silica leading edge preform were removed from cold storage and allowed to warm to room temperature. Miniature flow tests were performed on the leading edge preform to identify specific flow characteristics. The leading edge, two side panels, and the back panel were loaded into the compression mold and the graphite epoxy substructure was loaded inside the ablative structure. The entire heat shield and graphite epoxy substructures were cocured in the steel cavity section compression mold at 350°F for two hours in one operation (Figure 2.4-1). Figure 2.5.1-5 shows the cocured structure after net molding.

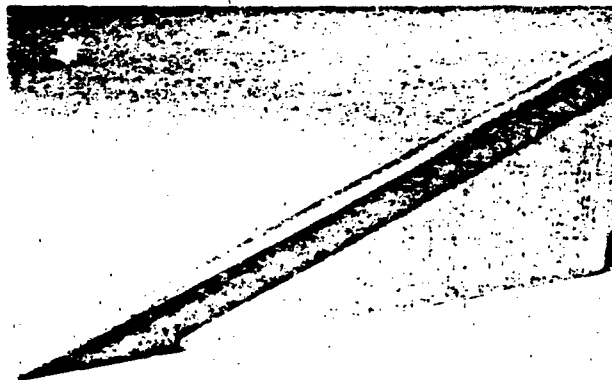


Figure 2.5.1-5. Net Molded and Cocured Structure

The net molding operation, representing a substantial cost saving in itself, also provides details that are primary bonded together. This approach eliminated 1) the need for a separate compression mold for the leading edge, 2) separate curing of the ablative side panels, 3) preparing the ablative material for subsequent bonding operations, and 4) secondary side panel routing and bonding operations.

Honeycomb Core

The phenolic honeycomb core (HRP 3/16-5.5) (Figure 2.5.1-6), which provides the necessary shear stiffness to the air vane, was obtained from the Hexcel Corporation. After dimensional inspection of the honeycomb core, the torque box pocket area was grit blasted and primed. Foaming adhesive HT424 was applied to the inside of the torque box pocket area and the basic honeycomb structures, forward and aft, and were bonded in place (Figure 2.5.1-7). Then the honeycomb was machined to its final configuration (Figure 2.5.1-8).

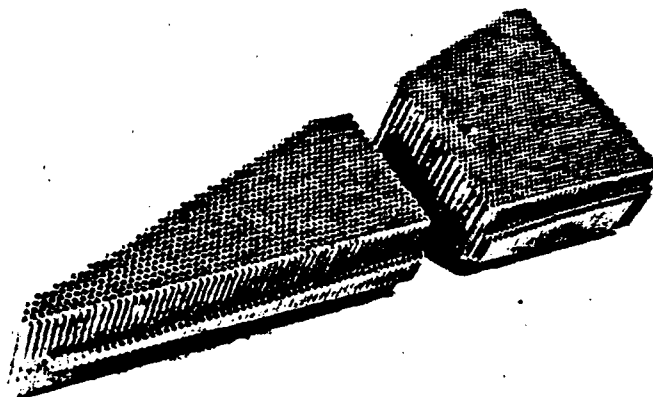


Figure 2.5.1-6. Honeycomb Core Prior to Final Machining

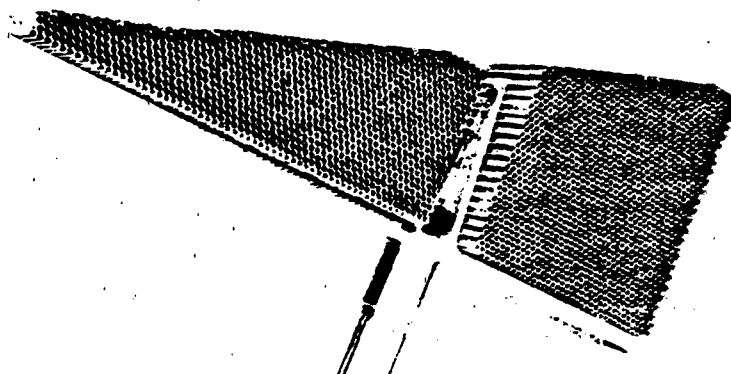


Figure 2.5.1-7. Honeycomb Core Positioned in Torque Box Pocket Area

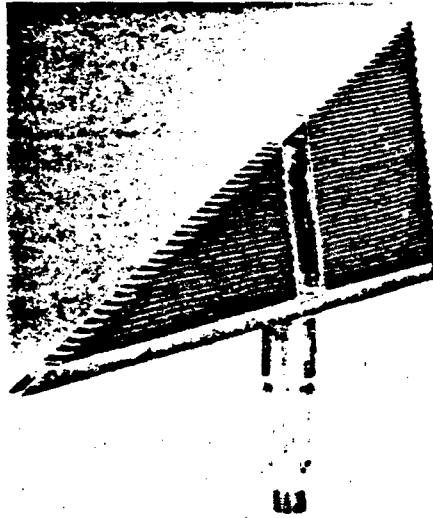


Figure 2.5.1-8. Honeycomb Core Bonded and Machined in Torque Box

Carbon Phenolic

The seal is formed from plies of carbon phenolic broadgoods that have been stacked and compression molded at 350°F for five hours. The individual graphite seals were machined at an angle that gives the required end grain fiber orientation needed for the seal to survive reentry heat.

Secondary Operations

The cocured composite/heat shield structure was bonded to the honeycomb torque box assembly using the matched metal bonding fixture. Film adhesive HT424 was placed between the two structures and the cure cycle used was 40 psi for 60 minutes at 340°F. Concurrently, the two bottom heat shield panels were primary bonded to the grit blasted, vapor degreased metallic structure (see Figures 2.5.1-9 and 2.5.1-10).

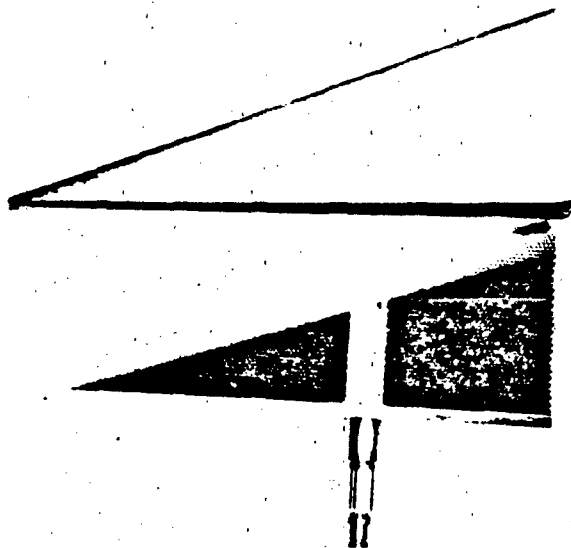


Figure 2.5.1-9. Prefit for Final Bonding of Honeycomb Torque Box to Cocured Structure

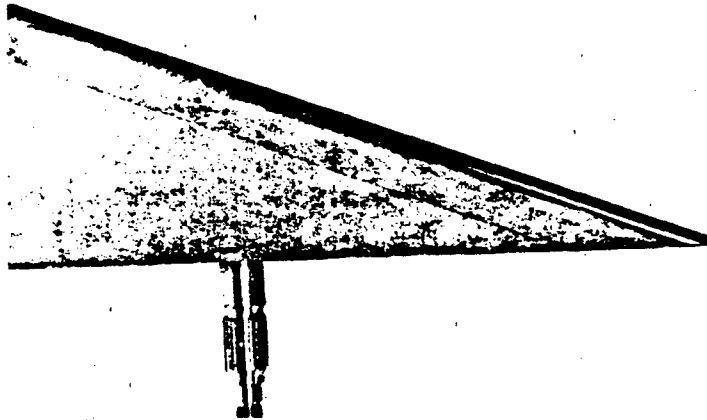


Figure 2.5.1-10. Final Composite Airvane Assembly

The previously fabricated carbon phenolic seal was mounted in the PII ED bonding fixture and bonded to the shaft of the air vane assembly. The assembly was then cured at 340° for 30 minutes. See Figure 2.5.1-11 for process flow plan.

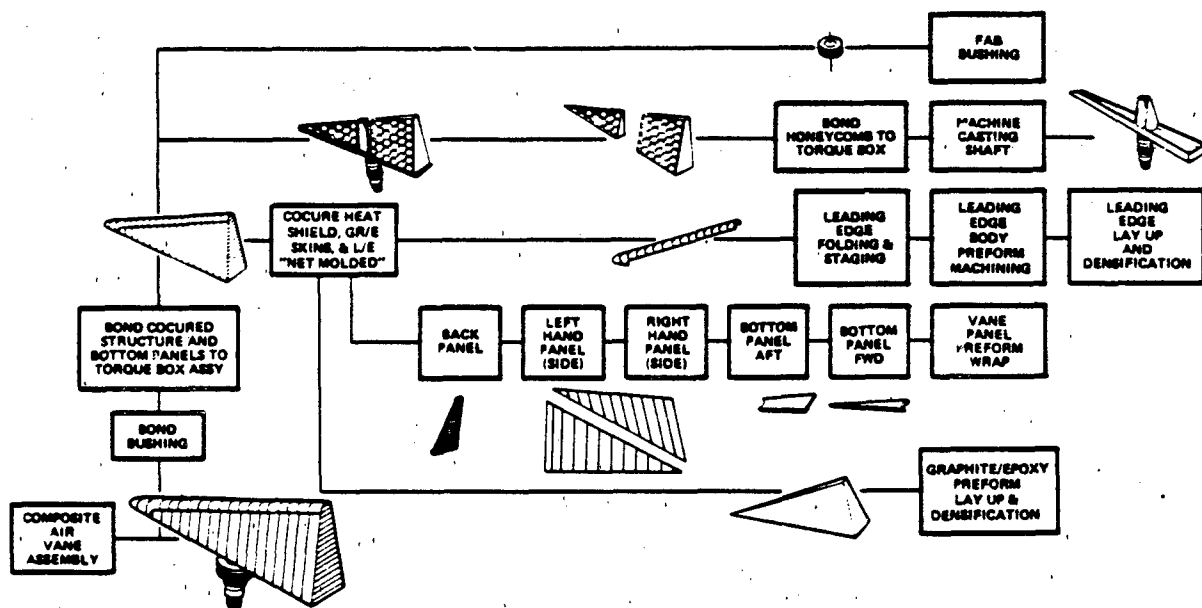


Figure 2.5.1-11. Process Flow Plan

2.5.2 Static Test Results

The first static test article of the composite air vane was tested on July 31, 1981. The test setup, instrumentation, and loading condition were in accordance with the static test plan, Martin Marietta document TPL 10200012-001 Revision A. During the loading sequence, we observed that at 80 percent DLL all the rubber loading pads began to slip along the loading face of the vane toward the leading edge. At 140 percent DLL the test was stopped because of excessive slippage of the loading pads which caused high stresses and deformations. Accordingly, test data and results were judged invalid and are not reported.

The test fixture and loading pads were modified so the pads would not slip. A second test article was fabricated and static tested on August 27, 1981, following the same procedures established in the test plan.

In addition to the five deflection measurements on the vane as described in the test plan, dial gages were installed to measure the deformation of this test fixture. The net vane deflections were then calculated by subtracting the fixture deformation from the vane deflection readings. The deflection data are compiled in Table 2.5.2-I.

TABLE 2.5.2-I

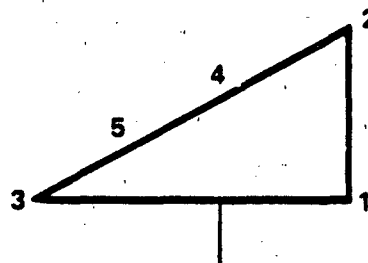
Deflection at 100 Percent Design Limit Load

DCDT NO.*	Total Deflect. (IN)	Fixture Deform. (IN)	Test Net Deflect. (IN)	Analysis Deflect. (IN)
1.	-.0110	-.0013	-.0097	-.008
2.	-.2301	-.0132	-.2169	-.101
3.	-.2657	-.0013	-.2644	-.158
4.	-.1085	-.0083	-.1002	-.045
5.	-.1294	-.005	-.1244	-.074

* See Figure 2.5.2-1 for Actual DCDT Locations.

The table shows the vane deflections at 100 percent DLL at the designated locations of DCDTs given in Figure 2.5.2-1. The fixture deformations and net deflections are given. The deflections based on NASTRAN analysis are shown at the corresponding locations for comparison.

Figure 2.5.2-1. DCDT LOCATIONS



The test results indicate that the test vane is not as stiff as the analysis predicted. At the base for points 1 and 3, the flexibility factors are 1.21 and 1.67 respectively. Along the leading edge at points

2, 4, and 5, the corresponding flexibility factors are 2.15, 2.23, and 1.68.

It is postulated that the larger test deflections could be the result of the three conditions listed below:

- 1 The analysis model did not include the bondline which would contribute to the flexibility.
- 2 The elastic properties of the shell could be lower in the test article than those used in the analysis.
- 3 The test loads were applied by means of four loading pads; whereas the analysis used load distribution over the entire surface.

The strain data were taken at the vane surface and at the steel torque section as depicted in Figure 2.5.2-2. The strain data were transformed to stress components in the X and Y directions and the corresponding shear stresses by applying the appropriate constitutive equations to the resulting stresses at 100 percent DLL, as shown in Table 2.5.2-II. The stresses predicted by NASTRAN analysis are included in Table 2.5.2-III.

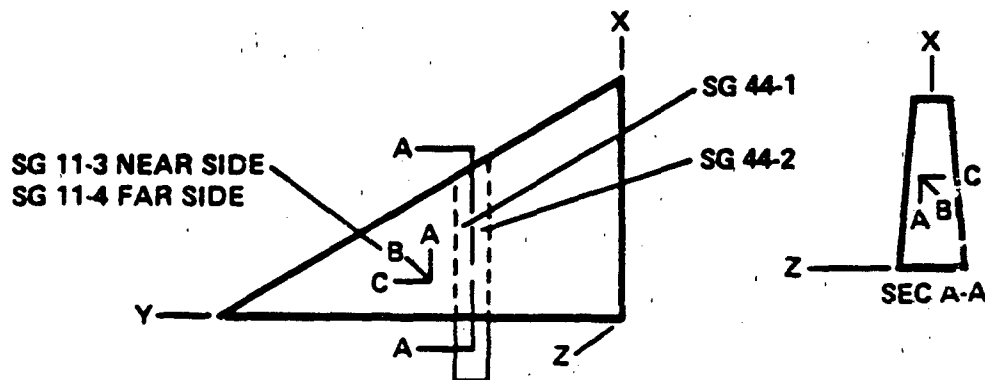


Figure 2.5.2-2. Strain Gage Designations

TABLE 2.5.2-II

Stress Components - Test

Gage No.	σ_x (Psi)	σ_y (Psi)	σ_z (Psi)	T_{xy} (Psi)	T_{xz} (Psi)
11-3	1853	2212	-	-1336	-
11-4	-1918	-2282	-	-1518	-
44-1	20269	-	5969	-	6992
44-2	22090	-	6397	-	6631

TABLE 2.5.2-III
Stress Components - Analysis

Gage No.	Element No.	σ_x (Psi)	σ_y (Psi)	σ_z (Psi)	T_{xy} (Psi)	T_{xz} (Psi)
11-3	220	3109	4487	---	-950	---
11-4	620	-3127	-4493	---	538	---
44-1	865	5459	---	272	---	1820
44-2	855	4595	---	2863	---	1991

The comparison of the test and analysis data showed that the stresses in the shell from the test were lower than those from analysis and the reverse was true for the stresses in the steel torque section. It is postulated that the bond between the graphite laminate and the steel channel in the test vane did not provide a rigid load path as compared to the torque section. As a result, the stresses are higher in the steel ribs than those predicted by analysis. The analytical model did not include the bond layer, so a rigid load path exists to transfer load to the shaft.

The test loads were increased by 20 percent DLL until 200 percent DLL was reached. No structural failure was detected.

APPENDIX A

Composite Air Vane
Thermal Analysis



A-1 INTRODUCTION

The thermal analysis of the composite air vane has been completed and the ablative heatshield sized to meet the relatively harsh thermal and rain environment of the Pershing II reentry. The vane concept as analyzed features an advanced composite substructure which is cocured with the ablative heatshield in a unique process expected to yield a lower cost air vane than the stainless steel air vane currently planned for use on the PII RV. The substructure material is graphite epoxy and the heatshield material which was selected for use and which is compatible with the cocure process is rubber modified silica phenolic (RMSP 1/2:1). The epoxy resin in the graphite/epoxy composite has a useful temperature limit of 350°F. Four distinct sections of the vane were analyzed: the leading edge, side panels, root chord, and trailing edge. Ablative thicknesses were sized appropriately for each section to prevent the graphite epoxy substructure from exceeding 400°F before the end of the flight. Worst case assumptions were used in this analysis and included: stagnation heating with no vane deflection for the leading edge; vane deflection for the side panel; heating augmentation varying from 1.0 to 4.7, due to the gap between vane bottom and vane pad for the root chord; and heating on the trailing edge which was assumed to be 56 percent of the side panel heating. Rain erosion was predicted for the leading edge and side panels, but not for the root chord and trailing edge since it was considered that they would be shielded from direct impact of rain due to their orientation. The method of analysis, results, and conclusions/recommendations follow.

II. METHOD OF ANALYSIS

A thermal analysis of the composite air vane was performed to size the ablative heatshield. The object of this analysis was to accurately predict maximum material recessions for each section of the vane, owing to a worst case thermal environment and to rain erosion, and yet to have enough thermal insulation remaining to prevent the graphite epoxy substructure temperature from exceeding 350°F before the end of the flight.

The thermal design trajectory used in this analysis was the same as used for the PII RV (body) heatshield (References 1 and 2). Since it was found in the RV heatshield analysis that bulk temperatures of ablative and substructure are 210°F at the start of reentry, this value was assumed for the vane analysis.

A. Leading Edge

Leading edge cold wall heating rates were determined first by using the FO-070 portion of the FO-086 one dimensional aero heating program, for a body angle of 3.3 degrees and body angle of attack as defined in the thermal design trajectory. The resulting local flow was used in the Beckwith and Gallagher method of FO-086 to predict heating due to stagnation pressures (Figure A-1) for the vane sweep angle of 69.75 degrees and leading edge radius of 0.50 inch. The TCAP-III thermo-chemical ablation program was then applied, using the predicted cold wall heating values (Figure A-2) to model the thermal recession and rain erosion. No vane deflection (versus time) was considered in this portion of the analysis since this was believed to be more conservative.

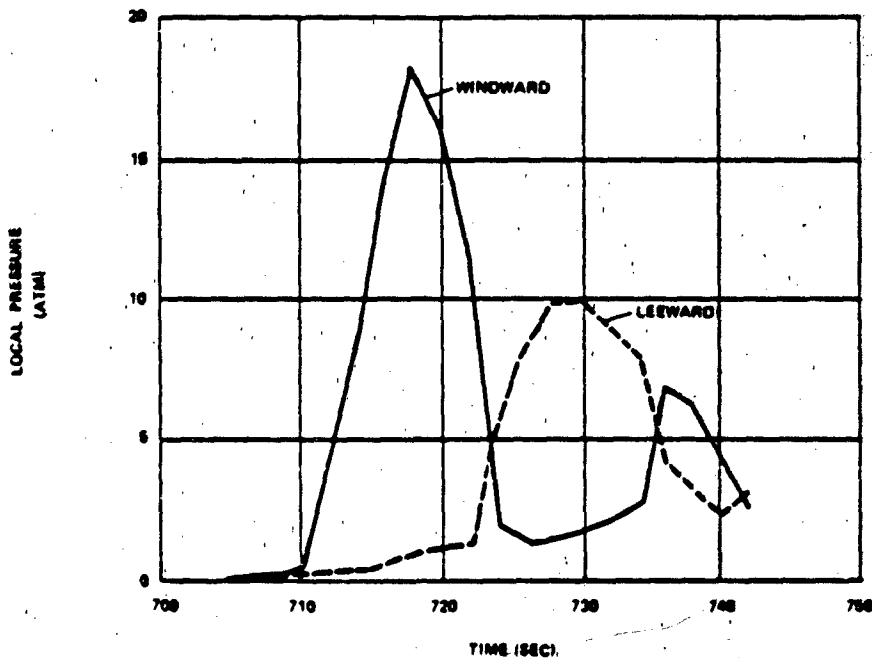


Figure A-1. RV Vane Leading Edge Local Pressure

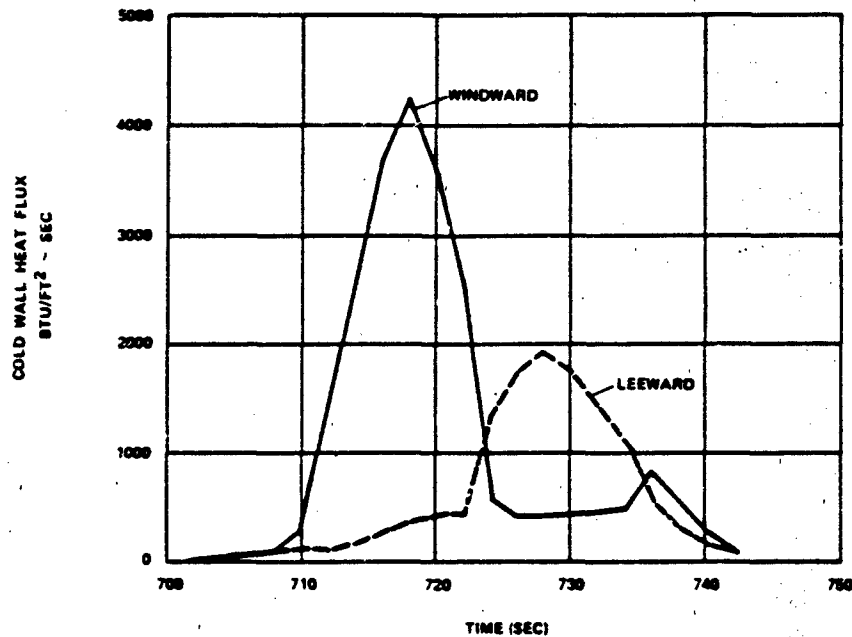


Figure A-2. Vane Leading Edge Cold Wall Heat Flux

The ablative material on the leading edge is silica phenolic, the same material as used for the PII RV air vane leading edge, and is formed with a 30-degree shingle angle wrap (0.50 inch radius, 0.6 inch thickness). The 30-degree shingle wrap was chosen to better absorb the thermal and rain erosion. The thermophysical and rain erosion resistance parameters for silica phenolic are shown in Table A-1 and Figure A-3 respectively.

Table A-1

Silica Phenolic Thermal Properties

CONDUCTIVITY (Btu/in-sec R)			SPECIFIC HEAT (Btu/lbm-R)		
TEMPERATURE (R)	VIRGIN PLASTIC	CHAR	TEMPERATURE (R)	VIRGIN PLASTIC	CHAR
0	6.40×10^{-6}	3.35×10^{-6}	540	0.223	0.178
500	6.40×10^{-6}	3.33×10^{-6}	1440	0.3035	0.289
1440	6.40×10^{-6}	3.33×10^{-6}	1800	0.2925	0.272
2060	6.40×10^{-6}	7.50×10^{-6}	3600	0.31	0.361
7460	6.40×10^{-6}	1.17×10^{-5}	10000	0.31	0.361
10000	6.40×10^{-6}	1.17×10^{-5}			
EMISSIVITY			VIRGIN PLASTIC DENSITY (lb/cu.in) 0.0578		
TEMPERATURE (R)	VIRGIN PLASTIC	CHAR	CHAR DENSITY (lb/cu.in) 0.0437		
0	0.75	0.75	MOLECULAR WEIGHT OF		
3600	0.75	0.75	DECOMPOSITION CASES 56.0		
3700	0.75	0.50	HEAT DEPOLYMERIZATION 155.0		
10000	0.75	0.50	RESIN FRACTION 0.244		
HEINSON-SPINDLER COEFFICIENTS			REACTION ORDER 3.0		
$\epsilon = aT^{-b} e^{(-c/T)}$					
a = 2.22×10^{10}					
b = 0.5					
c = 1.16×10^3					

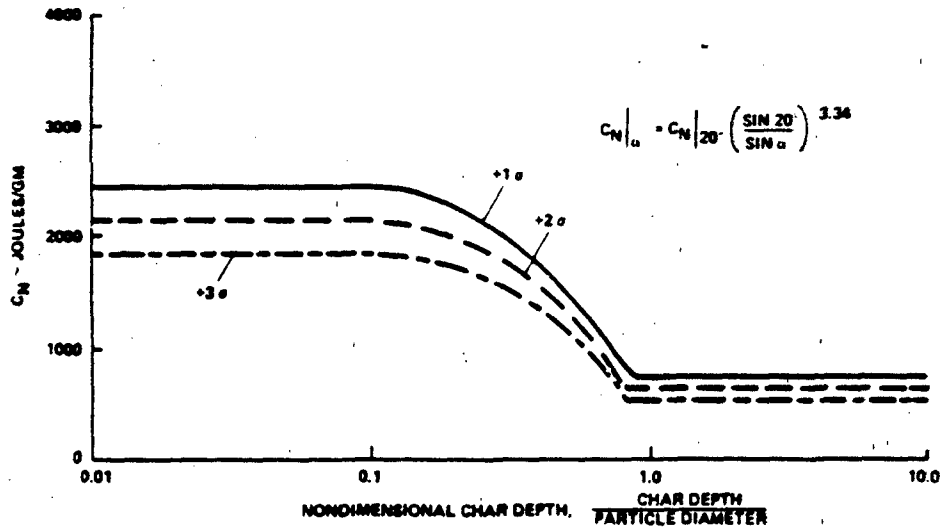


Figure A-3. Silica Phenolic Rain Erosion Resistance

B. Side Panel

Local flow on the vane side panel was determined using a Patriot vane flow program (Reference 3) in which body angle of attack, vane wedge angle, and vane deflection were considered. The body angle of attack and vane deflection histories are shown in Figure A-4. Cold wall heating rates (Figure A-5) were then calculated using the flat plate option of FO-086. The Eckert reference temperature method was used to determine the heat transfer coefficients and the flow was assumed to be turbulent. The skin friction correlation was based on the Blasius method for adiabatic wall temperatures less than 3400°R, and the Shultz-Grunow method for higher temperatures. The recovery factor was assumed to be 0.90. Thermal recession and rain erosion values were predicted using the TCA2-III program.

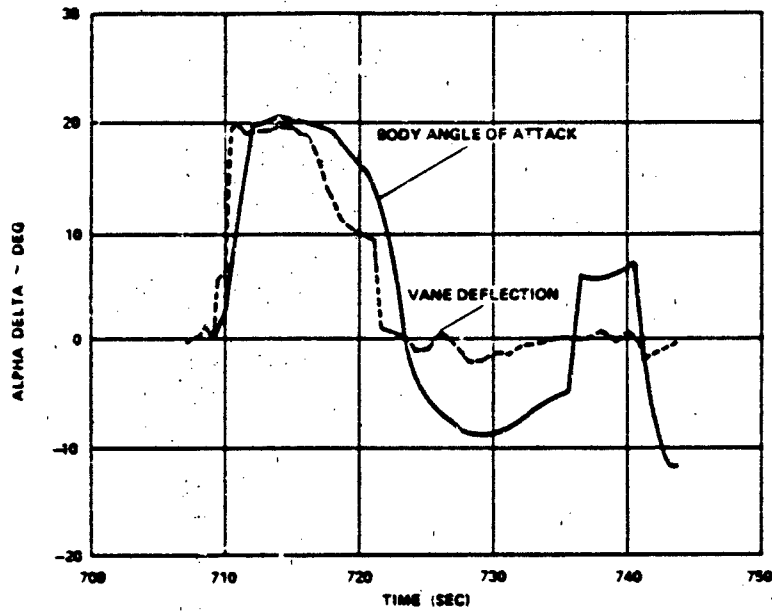


Figure A-4. RV Vane Deflection and Angle of Attack versus Time

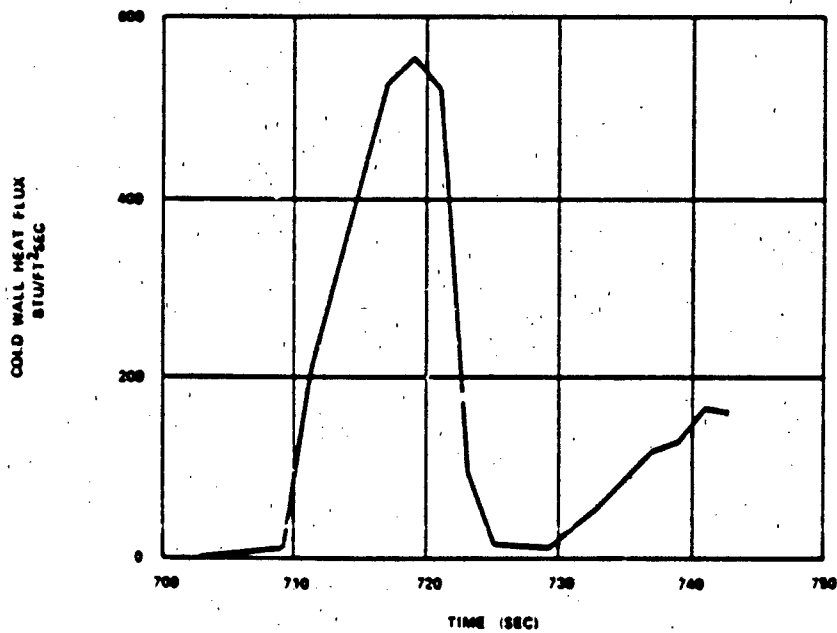


Figure A-5. RV Vane Side Panel Cold Wall Heat Flux

The material used for the side panel heatshield is RMSP (1/2:1), the same material as used for the PII RV body heatshield, and also used on the vane root chord panel and trailing edge surfaces as well. The thermo-physical properties and rain erosion resistance parameter are shown in Table A-II and Figure A-6. The thermal properties for the backup structure (graphite epoxy) are shown in Table A-III.

TABLE A-II

Rubber Modified Silica Pheholic (RMSP-1/2) Thermal Properties

CONDUCTIVITY (Stu/la-sec R)			SPECIFIC HEAT (Stu/Lbm- R)		
TEMPERATURE (R)	VIRGIN PLASTIC	CHAR	TEMPERATURE (R)	VIRGIN PLASTIC	CHAR
0.0	3.175X10 ⁻⁶	3.71X10 ⁻⁶	0.0	0.20	0.178
2480.	3.175X10 ⁻⁶	3.71X10 ⁻⁶	1440.	0.3055	0.289
3200	3.175X10 ⁻⁶	6.95X10 ⁻⁶	1800.	0.2925	0.272
3460	3.175X10 ⁻⁶	1.0X10 ⁻⁵	3600.	0.31	0.361
10000.	3.175X10 ⁻⁶	1.0X10 ⁻⁵	10000.	0.31	0.361
	EMISSIVITY		VIRGIN PLASTIC DENSITY (lb/cu. in)		
	VIRGIN PLASTIC	CHAR	CHAR DENSITY (lb/cu. in)		
0.0	0.75	0.75	MOLECULAR WGT. OF DECOMPOSITION GASES		
3600.	0.75	0.75	HEAT OF DEPOLYMERIZATION		
3700.	0.75	0.50	RESIN FRACTION		
10000.	0.75	0.50	REACTION ORDER		
	NUMERICAL SPINDLER COEFFICIENTS -D (-C/T)				
	S = AT e				
	A = 2.105 x 10 ¹⁶				
	B = 0.5				
	C = 1.76x10 ⁵				

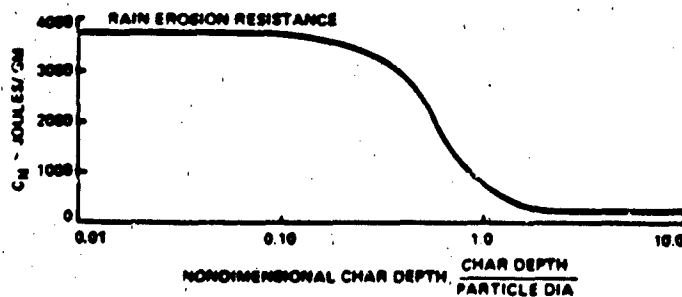


Figure A-6. Rain Erosion Resistance

TABLE A-III

Graphite/Epoxy Thermal Properties

Density 0.058 lb/in ³	
Conductivity (Btu/in sec ⁸ R)	
<u>Temperature (°R)</u>	
600	1.058x10 ⁻⁵
800	1.124x10 ⁻⁵
900	1.157x10 ⁻⁵
Specific Heat (Btu/lbm °R)	
<u>Temperature (°R)</u>	
600	0.245
800	0.308
900	0.339

C. Root Chord

The flow pattern which will exist in the gap between the vane bottom and the vane pad is extremely complex and does not lend itself readily to analytical modeling. Wind tunnel data obtained for the 15 and 30 percent PII RV scale models indicate peak pressure ratios (local pressure measured under vane to body local pressure just upstream) which vary from 1.0 to 3.1 with increasing angle of attack and no vane deflection. With large vane deflection (about 20 degrees) the measured pressure ratios reach a maximum of 3.3 at 15 degree angle of attack and then drop off as angle of attack continues to increase. Reference 4 suggests that heat augmentation, which varies from 3.4 to 4.7 times the local body heat flux, will exist in this gap, particularly in front of the shaft, where near stagnation conditions will occur. Since the PII wind tunnel data have not been fully reduced, the root chord heatshield has been sized for the augmentation factor range of 3.4 to 4.7. The resulting heat flux values used on the root chord are shown in Figure A-7.

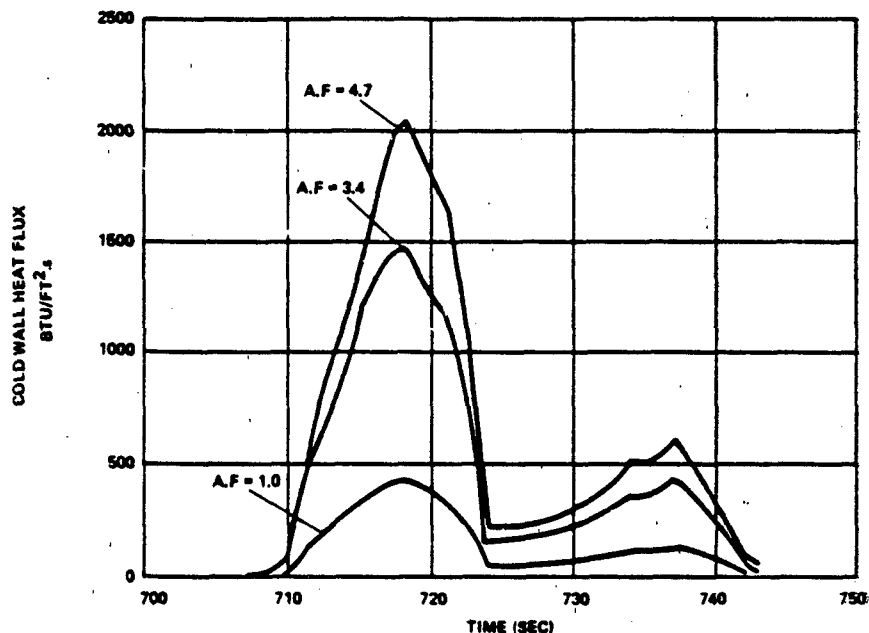


Figure A-7. Root Chord Cold Wall Heat Flux

The backup structure for the root chord is 17-4PH stainless steel, which can reach temperatures as high as 600-800°F without significant degradation of the material strength properties. However, since the graphite epoxy side panel skins must be bonded to the casting channel legs, as shown in Figure A-8, allowing the casting temperature to reach this range could cause the bondline to exceed its strength critical value of 400°F. Therefore, a three dimensional SINDA model (Figure A-8) of the root chord/shaft region of the vane was constructed and exercised to determine the effect of allowing the root chord casting (floor) to reach as high a temperature as possible without exceeding the bondline temperature limit. The range of application of the various augmentation factors, shown in Figure A-8, was determined through a combination of hypersonic wind tunnel data and the vane deflection versus time history.

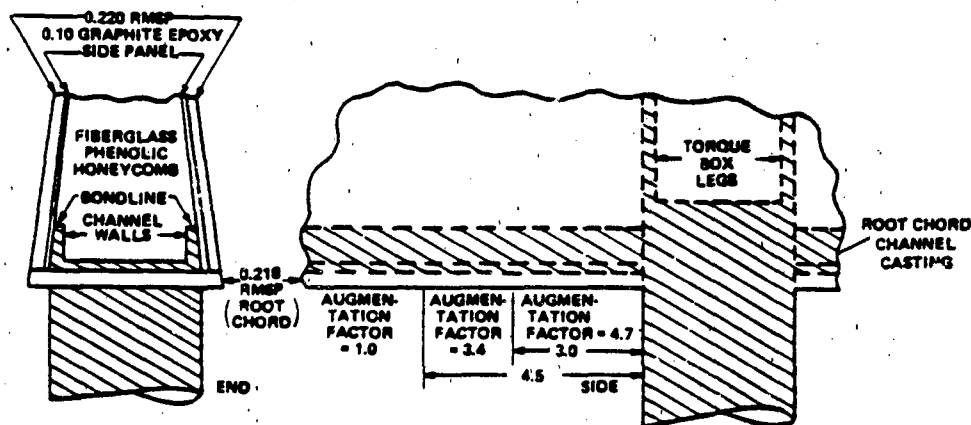


Figure A-8. Three Dimensional Root Chord Casting

D. Trailing Edge

The trailing edge of the RV air vane is not subjected to either high heating or erosion by rain. The heating on this portion of the vane (Figure A-9) is assumed to be 56 percent of the side panel heating which is a value consistent with turbulent separated flow around bluff bodies.

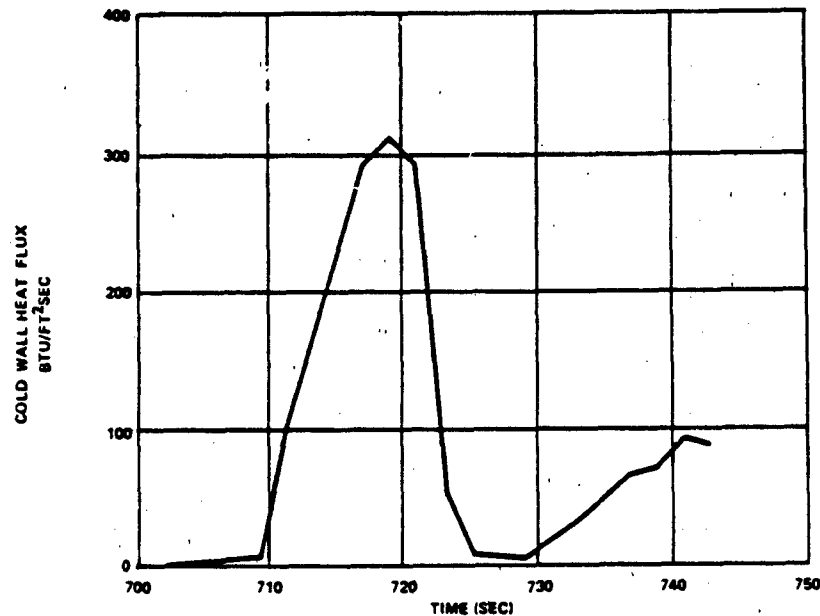


Figure A-9. RV Fin Trailing Edge Cold Wall Heat Flux

III. RESULTS

The PII RV reenters the earth's atmosphere with the vanes in an "X" configuration (wind vector centered between the bottom pair of vanes) and the initial maneuver is a pull up with 20 degree angle of attack held for approximately six seconds. During this portion of reentry, the windward (bottom) pair of vanes are exposed to very high heating while the leeward (top) pair of vanes are in the shadow of the RV. Following this is a pull down maneuver which exposes the top pair of vanes to the wind, but due to the decreased speed, the heating during this portion of reentry is not nearly as severe as it was for the bottom pair during the pull up. As a result, the leading edges of the bottom pair of vanes experience a greater amount of thermally induced recession than the top pair, having a dramatic impact on the vane effectiveness due to the differential loss of planform area.

The peak local pressure on the leading edge, (about 18 atmospheres) causes the heat flux to be in excess of 4000 Btu/ft²-sec. The predicted surface temperature and silica phenolic/graphite epoxy interface temperature responses are shown in Figures A-10 and A-11 respectively. Note that the interface temperature reaches a peak of 350°F at the end of the flight, which is below the bond critical temperature limit. The predicted recession for the windward vane leading edge is shown in Figure A-12, where it is apparent that half of the total recession is due to rain erosion. This result is based on +3σ values of rain erosion data for the silica phenolic material (Reference 5), and is believed to be quite conservative.

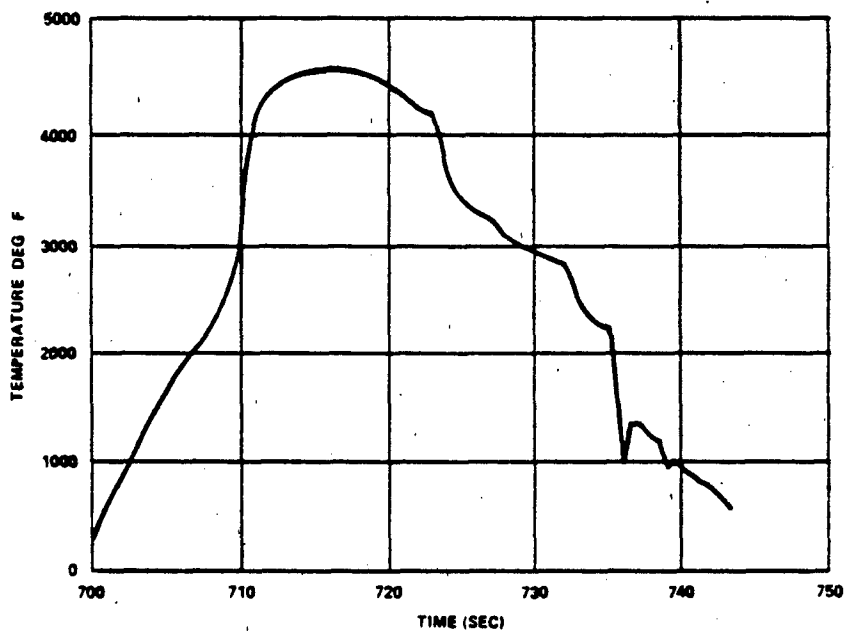


Figure A-10. Vane Leading Edge Surface Temperature

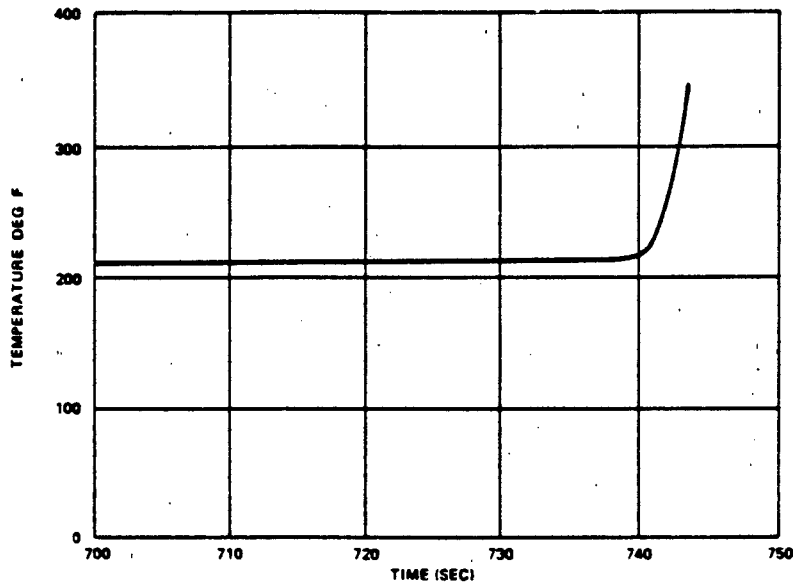


Figure A-11. Leading Edge Backside Temperature Response

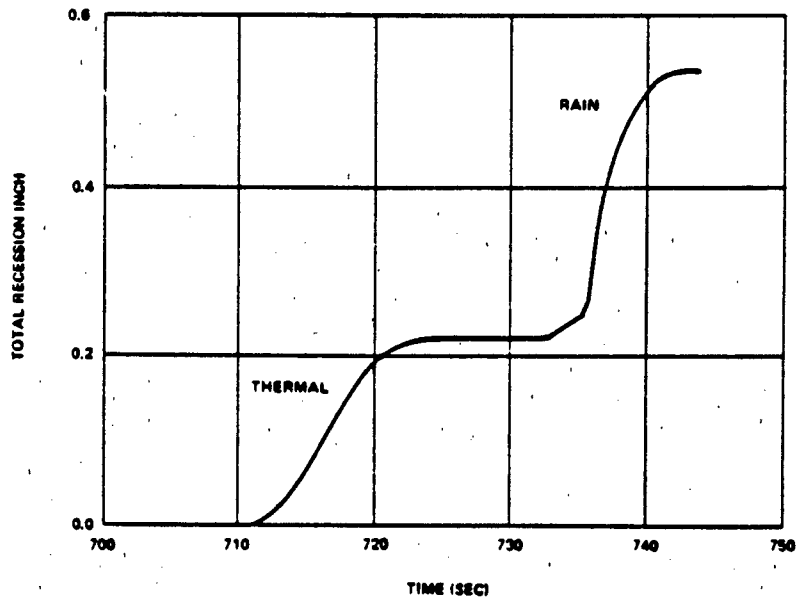


Figure A-12. Leading Edge Total Recession

The predicted recession for the side panels (0.240 RMSP/0.10 graphite epoxy) is shown in Figure A-13. The resulting interface (bondline) temperature is shown in Figure A-14, for a point immediately behind the leading edge (highest heating), and a point closer to the root chord in the vicinity of the vane shaft. The 35°F bondline temperature difference is due to an approximate 10 percent decrease in heating, which is typical for increasing watted length (further back on the vane body). The forward point actually sized the thickness of heatshield required for the side panel, but the later point was done for the purpose of the three dimensional root chord model.

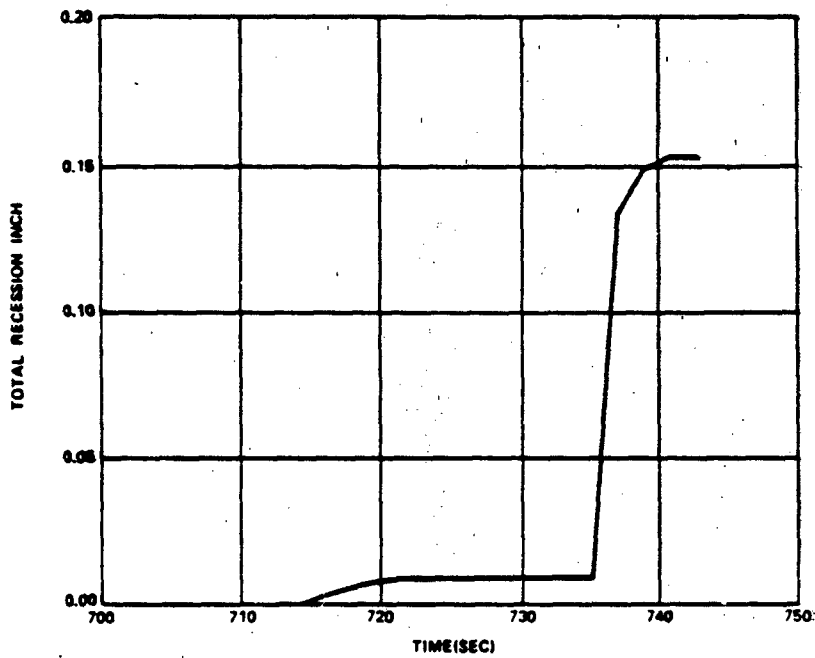


Figure A-13. Vane Side Panel Ablative Recession

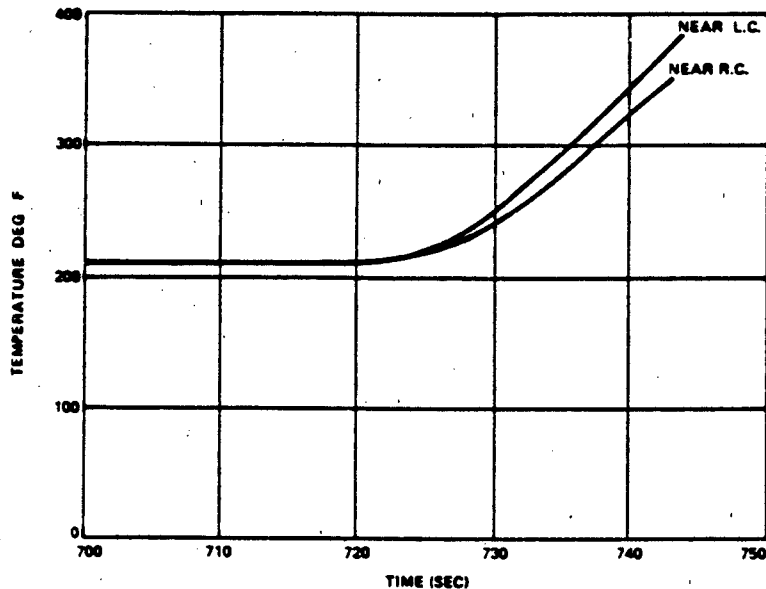


Figure A-14. Side Panel Bondline Thermal Recession

The recessions predicted for the various augmentation areas of the root chord are shown in Figure A-15. These recession values do not include the effects of rain erosion since it is believed that this region of the vane would be shielded from direct impingement. The one-dimensional (TCAP-III) analysis bondline temperatures are shown in Figure A-16. Note that there is approximately 150°F difference between each of the augmentation areas at the end of flight because of the constant thickness (0.218 inch) of the heatshield in each of the areas. These temperatures, together with the temperatures generated for the side wall were used in the three-dimensional root chord model to determine the ultimate graphite epoxy/casting interface temperature in the region of the channel casting walls. The results for this portion of the analysis are shown in Figure A-17 for the portion of the casting wall that reached the highest temperature (390°F).

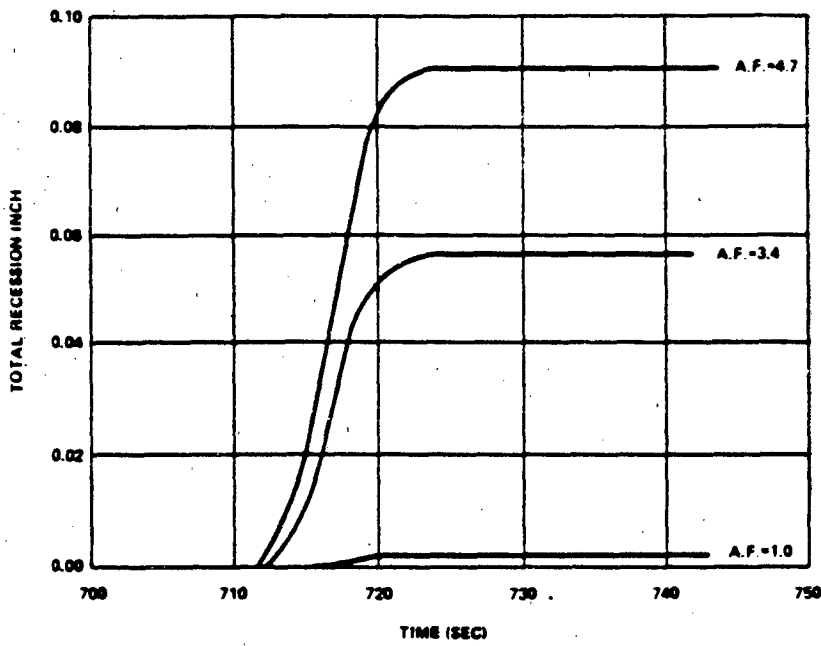


Figure A-15. Root Chord Total Thermal Recession

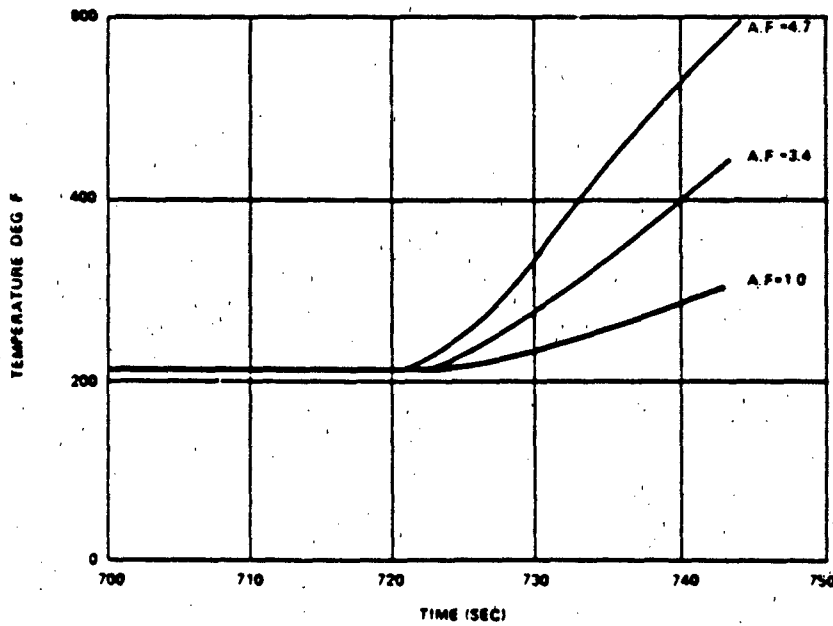


Figure A-16. Root Chord Bondline Temperature Response

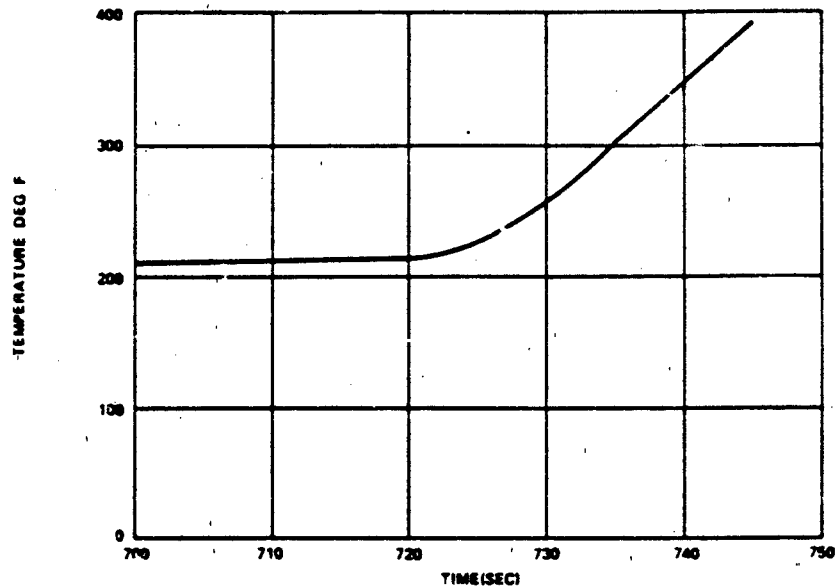


Figure A-17. Graphite Epoxy/Root Chord Stainless Steel

This implies that the 600°F temperature of the root chord floor (in the 4.7 augmentation factor area) should not adversely affect the bondline temperature on the casting channel walls and that selecting the minimum thickness heatshield 0.218 inch (assumed constant over the entire length of the root chord) was a valid selection. The small area of the root chord bondline (approximately three inches in front of the shaft) which exceeds 400°F for the final 10 seconds of flight will cause local debonding. However, we believe that this will not be a serious problem since the very phenomenon that causes the high heating (i.e., very high pressure) will tend to hold the heatshield in place. Furthermore, there is 0.127 inch of RMSF remaining in this area, of which 10 percent is virgin plastic at the backside.

The heating on the vane trailing edge is mild (56 percent of the side wall heating) in comparison to the other sections. The cold wall heat flux shown in Figure 8 causes less than 0.001 inch of surface recession, and since rain erosion was not considered for this portion, it was found that 0.217 inch of RMSF would be adequate to protect the bondline to 350°F as shown in Figure A-18.

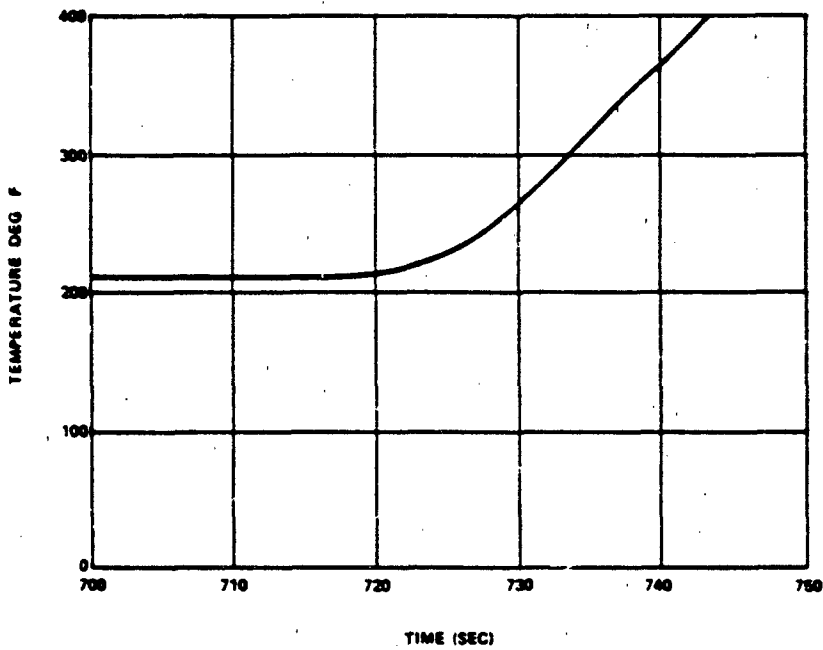


Figure A-18. Trailing Edge Bondline Temperature Response

A-4 CONCLUSION/RECOMMENDATIONS

The thermal analysis of the composite RV air vane is completed, the required ablative thicknesses defined, and both are summarized in Table A-IV. The only area of the vane that may cause problems in flight is the highest augmented heating area assumed on the root chord, where bondline temperatures are predicted to exceed 400°F during the later portion of reentry. It is suggested that bonding agent mechanical properties versus temperature be reviewed since it is known that certain adhesives (i.e., HT-424) are capable of withstanding higher than cure temperature for a brief period without serious degradation of bond strength. Otherwise, no other significant thermal problems are anticipated for the composite vane on the PII RV.

Table A-IV

Composite Airvane Heatshielded Sizing Summary

Vane Section	Leading Edge	Side Panel	Root Chord	Trailing
Substructure Thickness (in)	Graphite Epoxy/0.10	Graphite Epoxy/0.10	Stainless Steel/0.10	Graphite Epoxy/0.10
Heatshield Material	Silica Phenolic	RHSP	RHSP	RHSP
Thickness Required Due to:				
Thermal Recession (in)	0.220	0.007	0.089	0.001
Wear Erosion (in)	0.350	0.146	N/A	N/A
Bondline/Substructure (in) (Max Temp, °F)	0.030 (350)	0.087 (350)	0.129 (300)	0.217 (350)
Minimum Thickness ¹ (in)	0.600 ²	0.240	0.218	0.217

Notes: 1) All heatshield thicknesses shown above are minimum. Nominal tolerance for heatshield layup is ± 0.010 -inch.

2) Radius is 0.50 inch.

APPENDIX A
REFERENCES

- 1 P2E ANA 12400000-001, "PII RV Heatshield Thermal Analysis", Martin Marietta, January 24, 1980.
- 2 P2E DRS 12800000-002, "Trajectory Performance Requirements", Martin Marietta, January 1980. (Confidential)
- 3 SDO ANA 10203012-005, "SAM-D Control Fin Local Flow Used to Predict The Side Panel Aerodynamic Heating Rates", Martin Marietta, December 16, 1974.
- 4 P21 ANA 10800012-001, "Preliminary Thermal Analysis of Pershing II Air Vane Pads", Martin Marietta, May 6, 1975.
- 5 P2E TRP 12400000-002, "Rain Erosion Test of Air Vane Leading Edge, Pad, and Ramp Material Candidates on Mach 5 Sled at Holloman AFB", Martin Marietta, September 16, 1980.

END

FILMED

5-85

DTIC